NASA CR-135023
CASD-NAS-76-015

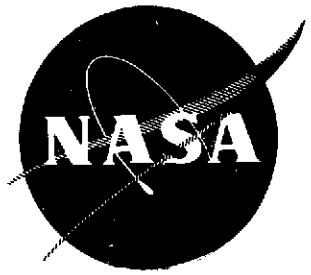

# AN ANALYTICAL STUDY OF REDUCED-GRAVITY FLOW DYNAMICS

April 1976

by
R. D. Bradshaw
J. L. Kramer
J. L. Zich

Prepared for
National Aeronautics and Space Administration
LEWIS RESEARCH CENTER
21000 Brookpark Road
Cleveland, Ohio 44135

Contract NAS3-17839

GENERAL DYNAMICS
*Convair Division*

(NASA-CR-135023) AN ANALYTICAL STUDY OF REDUCED-GRAVITY FLOW DYNAMICS (General Dynamics/Convair) 67 p HC $4.50 CSCL 20D

N76-24504

Unclas
G3/34 28185

NASA CR-135023
CASD-NAS-76-015

# AN ANALYTICAL STUDY OF REDUCED-GRAVITY FLOW DYNAMICS

April 1976

by
R. D. Bradshaw
J. L. Kramer
J. L. Zich

Prepared for
National Aeronautics and Space Administration
LEWIS RESEARCH CENTER
21000 Brookpark Road
Cleveland, Ohio 44135

Contract NAS3-17839

Prepared by
GENERAL DYNAMICS CONVAIR DIVISION
P.O. Box 80847
San Diego, California 92138

| 1. Report No. | 2. Government Accession No. | 3. Recipient's Catalog No. |
|---|---|---|
| NASA CR-135023 | | |

| 4. Title and Subtitle | 5. Report Date |
|---|---|
| AN ANALYTICAL STUDY OF REDUCED-GRAVITY FLOW DYNAMICS | April 1976 |
| | 6. Performing Organization Code |
| 7. Author(s) | 8. Performing Organization Report No. |
| Robert D. Bradshaw, James L. Kramer and Jon L. Zich | CASD-NAS-76-015 |
| | 10. Work Unit No. |
| 9. Performing Organization Name and Address | |
| General Dynamics Convair Division<br>P. O. Box 80847<br>San Diego, CA 92138 | 11. Contract or Grant No.<br>NAS3-17839 |
| | 13. Type of Report and Period Covered |
| 12. Sponsoring Agency Name and Address | Contractor Report |
| National Aeronautics and Space Administration<br>Washington, DC 20546 | 14. Sponsoring Agency Code |

15. Supplementary Notes

Project Manager, William J. Masica, Chemical Energy Division
NASA Lewis Research Center, Cleveland, CH 44135

16. Abstract

This study was conducted to add surface tension forces to a marker-and-cell code and to perform four incompressible fluid simulations in reduced-gravity. This marker-and-cell code has a variable grid capability with arbitrary curved boundaries and time-dependent acceleration fields. The surface tension logic includes a spline fit of surface marker particles as well as contact angle logic for straight and curved wall boundaries. Three types of flow motion were simulated with the improved code: impulsive settling in a model Centaur $LH_2$ tank, continuous settling in a model and full-scale Centaur $LO_2$ tank and mixing in a Centaur $LH_2$ tank. The impulsive settling case confirmed the NASA Lewis Research Center drop tower analysis which indicated more orderly fluid collection flow patterns with this method providing a potential savings in settling propellants. In the $LO_2$ tank, fluid collection and flow simulation into the thrust barrel were achieved; however, flow simulation of thin films along the bottom arbitrary curved boundary was inadequately modeled. The mixing simulation produced good results indicating both the development of the flow field and fluid interface behavior. The potential exists for examination of the influence of Bond number and mixer exit velocity on mixing time and fluid interface behavior.

| 17. Key Words (Suggested by Author(s)) | 18. Distribution Statement |
|---|---|
| Reduced Gravity, Settling, Mixing, Centaur, Marker and Cell, Incompressible Fluid Mechanics | Unclassified - Unlimited |

| 19. Security Classif. (of this report) | 20. Security Classif. (of this page) | 21. No. of Pages | 22. Price* |
|---|---|---|---|
| Unclassified | Unclassified | 63 | $3.00 |

*For sale by the National Technical Information Service, Springfield, Virginia 22151

# FOREWORD

This computer development and application study was conducted by General Dynamics Convair Division at San Diego under NASA Contract NAS3-17839. The research was accomplished under the direction of the NASA Project Manager, Mr. William J. Masica, NASA Lewis Research Center. The study was completed under the direction of Convair project leader, Dr. Robert D. Bradshaw with the scientific programming assistance of Mr. James L. Kramer and Mr. Jon L. Zich. Respective supervisory personnel were Mr. Robert E. Tatro, Chief of Thermodynamics and Mr. Roger E. Barnes, Chief of Engineering Software. The authors acknowledge the capable direction and assistance provided by Mr. Masica.

## ABSTRACT

This study was conducted to add surface tension forces to a marker-and-cell code and to perform four incompressible fluid simulations in reduced-gravity. This marker-and-cell code has a variable grid capability with arbitrary curved boundaries and time-dependent acceleration fields. The surface tension logic includes a spline fit of surface marker particles as well as contact angle logic for straight and curved wall boundaries. Three types of flow motion were simulated with the improved code: impulsive settling in a model Centaur $LH_2$ tank, continuous settling in a model and full-scale Centaur $LO_2$ tank and mixing in a Centaur $LH_2$ tank. The impulsive settling case confirmed the NASA Lewis Research Center drop tower analysis which indicated more orderly fluid collection flow patterns with this method providing a potential savings in settling propellants. In the $LO_2$ tank, fluid collection and flow simulation into the thrust barrel were achieved; however, flow simulation of thin films along the bottom arbitrary curved boundary was inadequately modeled. The mixing simulation produced good results indicating both the development of the flow field and fluid interface behavior. The potential exists for examination of the influence of Bond number and mixer exit velocity on mixing time and fluid interface behavior.


PRECEDING PAGE BLANK NOT FILMED

TABLE OF CONTENTS



PRECEDING PAGE BLANK NOT FILMED

LIST OF FIGURES





PRECEDING PAGE BLANK NOT FILMED

LIST OF FIGURES, Contd



LIST OF TABLES

## SUMMARY

Numerical simulations provide a valuable extension of drop tower tests to provide insight into fluid dynamic behavior in low-gravity environments. The purpose of this study was to simulate fluid behavior during settling in Centaur $LH_2$ and $LO_2$ tanks and to examine mixing flow in the Centaur $LH_2$ tank using the marker-and-cell code. To achieve this modeling in low-g the code required modification to include surface tension forces.

Initial attempts to include surface tension logic used a circular arc fit to obtain the radius of curvature. This approach was inadequate and necessitated going to the more complex spline fit for monotonic sequences. The monotonicity requirement of this approach was sometimes troublesome, however the method was more precise and the results were good. The single continuous interface has capability for different contact angles at each end where wall contact is made. The contact angle solution is usable with straight walls and concave or convex arbitrary boundary walls. The contact angle may be time dependent and is measured from the second or second last surface marker point from distances beyond the center of the adjacent boundary cell. The surface tension logic is basically superimposed on the surface marker particle logic which includes adding or deleting particles and interface smoothing. The surface tension force is defined as a pressure at the intersection of the interface and a line through cell centers but is translated to act and to be stored at the center of the surface cells. The method was verified with known geometric shapes where the radius of curvature was analytically available and was further verified with a test case involving fluid motion. The surface tension logic was then used on the four cases examined in this study.

A second computer code improvement concerned the convergence scheme. The code requires extensive iterations to converge in relatively full tanks when the gradient in the pressure field is low in reduced-gravity fields, i.e., coast periods rather than settling. At this time, the pressure field gradient in the tank is quite low. Two new convergence methods were considered but were found to be less efficient than the existing method. Therefore, the existing method was improved through an extrapolation technique which advances the pressure field one large step every 40 iterations. This method possessed stability and in all instances reduced the time for convergence. The code was also compiled with the FTN compiler to increase efficiency.

Three types of flow simulation were specified under this study. Case 1 involved impulsive settling with a Centaur model $LH_2$ tank, Cases 2 and 3 considered continuous settling in the Centaur $LO_2$ tank while Case 4 simulated mixing in a full-scale Centaur $LH_2$ tank. Case 1 was studied to provide insight into the fluid dynamics during impulsive settling where a fluid is set in motion by the equivalent of 12 lbs full-scale

thrust for a brief period after which thrust is terminated and the fluid continues to collect aft. A Lewis Research Center drop tower test where thrust lasted 0.30 sec had indicated potential for reducing settling propellants and was simulated. The simulation initially progressed smoothly and flow moved down the side wall and into the corner. During the 0.30 sec thrust period and until 0.9 sec, simulation and drop tower results were alike. After this time in the simulation, liquid did not flow radially inward over the bulkhead but continued to collect in the lower corner. This was unlike drop tower results but not a serious deviation. Some 0.5 sec later, flow did continue toward the centerline but arrived 0.6 sec later than in the drop tower case. The flow velocities down the wall decreased in magnitude with time; overall behavior was as expected. Initial convergence difficulties in low-g made the simulation costly and it could not be continued until fluid motion ceased. Impulsive settling shows promise as a weight-saving approach to accomplish settling. Modeling can be improved if more rapid convergence can be achieved at low-g levels.

In the $LO_2$ tank the behavior of settling flow in the region of the thrust barrel was of particular interest. Drop tower results had been only partially successful because of the complexity of modeling flow into the thrust barrel and also the difficulty in observing this flow. The variable grid capability was extensively used in simulating the thrust barrel. Because of cylindrical symmetry, the holes in the thrust barrel were modeled with slits of equal area. The model case had 30 percent liquid present to represent a drop tower case, while the full-scale case contained 9 percent liquid to model a full-scale Centaur settling. Initial flow in both simulations proceeded down the wall in a smooth manner. In the model Case 2, the flow proceeded up along the side of the thrust barrel and flow passed through the slit at a sufficient rate to indicate thrust barrel filling in a reasonably brief time. In both cases, however, flow along the aft bulkhead was difficult to model because a thin film resulted in only surface cells; these often lacked full or surface neighbors and could not adequately transmit the flow and pressure field information along this boundary. In the full-scale Case 3, an attempt to improve the resolution with finer cell size was inadequate as the film was significantly thinner. The full-scale Case 3 proceeded only to covering of the thrust barrel holes and had to be discontinued because of erroneous velocities along the aft bulkhead. The current state of the model cannot adequately simulate the flow of the thin films on the curved boundary. During both these simulations, surface tension calculations were satisfactory and convergence occurred in a reasonable number of iterations.

Case 4 was a new area of investigation in marker-and-cell flow dynamics simulation. The use of a jet mixer in a low-g coast orbit was modeled for a full-scale Centaur $LH_2$ tank with 65 percent liquid present. A low velocity flow was aimed toward the interface from the submerged jet. Mixing correlations predicted a time of 2000 seconds to achieve steady-state and total mixing while the Weber and Froude number criteria used predicted that interface break-up should not occur. The velocity field was observed to develop smoothly in the tank and progress away from the mixer and across the interface. The entrained flow below the mixer was well defined. Interface velocities induced waves and interface instabilities but ullage break-up did not occur.

Mixing times appear to be less than predicted since steady-state flow at the interface had occurred by 700 sec. Flow patterns indicate stratification would have been destroyed. Unexpected convergence problems necessitated running this case at a Bond number of 100 with a flat interface. Cases with lower Bond number are also of considerable interest and, in view of Case 1 results at low Bond numbers, should be within the capability of the model. Overall results of this case were very nearly as expected. Since the flow field is changing only very slowly, the solution converged each time step in minimal iterations and the case provided a low cost simulation of 700 seconds of mixing in reduced-gravity.

This study indicated the potential for simulating mixing with the marker-and-cell code to evaluate mixing times and flow behavior at the surface. Future comparisons between drop tower results and model simulation would be useful in the verification of existing criteria for interface behavior. The surface tension capability affords an opportunity for analysis of behavior where this mechanism is controlling, however improvements in convergence methods are required for Bond numbers less than 10. The study also indicated a need for further code development in the treatment of thin films on arbitrary boundaries.

# 1

## INTRODUCTION

Many requirements on space missions involve the motion of propellant in a reduced gravity field. Drop tower tests are one method of gaining insight into this fluid behavior. A second method is numerical techniques such as the marker-and-cell computer code. These are both interim approaches until experimental space payloads are available. One reduced-gravity fluid behavior problem is the requirement to settle propellants to the aft end of a space vehicle tank prior to engine restart. During space coast in earth orbit, propellants collect forward due to atmospheric drag or retromaneuvers and present a settling requirement. Propellants aboard Centaur are settled with the application of a settling thrust from hydrogen peroxide motors. The pattern of fluid motion during settling is of interest to define the required settling times. The operation of a jet pump in a cryogenic propellant tank in reduced gravity is a second fluid problem. A fluid jet has been recommended for mixing the propellant to reduce pressure rise due to stratification at the vapor interface. The extension of one-g mixer data to low gravity conditions has raised some doubts however, and until very recently no low-g drop tower data was available in this area of reduced-gravity research.

The marker-and-cell technique provides a convenient analytical tool to simulate low-g fluid behavior and to define both flow and pressure fields as well as the time requirements for the motion. Visual presentations of the fluid location and the velocity field are provided as well as detailed printouts on the velocity and pressure field. In very low-g fields, the surface tension forces dominate the acceleration forces. Therefore, it was important to add logic to the program which solves for these forces on the interface, particularly for simulation of impulsive settling or of mixing where acceleration forces are much lower than experienced in normal continuous settling.

In each of the cases considered in this study, drop tower data were available for model tank configurations. This provides for verification of a numerical method which can then be used for analysis of full-scale simulations and for extension of simulations beyond the time-limits of drop tower experiments. The logic and capabilities of the code in its original form and the logic for the surface tension modifications are both outlined in this report, as well as simulation results.

PRECEDING PAGE BLANK NOT FILMED

# 2

## COMPUTER CODE DEVELOPMENT

The computer code development task in this study had two objectives; the modification of a marker-and-cell code to include surface tension and the improvement of convergence techniques in the code when simulating very low gravity fields. An existing marker-and-cell code, ERIE (Ref. 1-4) was used as a starting point for this modification. The initial code contained a variable-grid capability and was in overlay structure to reduce core storage.

The code is used to solve problems in incompressible fluid dynamics using an approach known as the Simplified Marker-and-Cell (SMAC) technique which was originated at Los Alamos Laboratory (Ref. 5). The cells provide a grid mesh for problem solution and liquid accountability with a specification of velocity and pressure fields; the particles indicate the fluid location. The newly improved code has the capability for modeling surface tension pressure, arbitrary boundaries, and variable gravity fields.

In order to acquaint the reader with the basic approach to the computer logic and to provide stand alone capability for this document, a few pages from Reference 1 are summarized to present further insight into the marker-and-cell approach prior to describing modifications current to this contract. For the reader interested in greater detail on the program logic, a current program documentation is provided in Reference 6.

The SMAC method is a numerical finite difference technique for solution of the Navier-Stokes equations of motion for incompressible viscous fluid flow. The method solves the complete Navier-Stokes equations giving a time-dependent solution. The method is applicable to confined flow or free surface flow. The SMAC method overlays the fluid with a two-dimensional rectangular grid mesh in either rectangular or cylindrical coordinates. Horizontal velocities are defined at the midpoints of each side of each rectangular element while vertical velocities are defined at the midpoints of the top and bottom sides. Finite velocities are defined each time step only for cells which are full or surface; the latter being those next to an empty cell. Various designations are given to other cells in the grid depending on their location and function as shown in Figure 1. Velocities satisfy tangential and normal stresses on surface cells.

A pressure field is defined throughout the fluid with the pressure defined at the center of each full cell. The pressures on surface cells are interpolated to satisfy the normal stress condition plus a surface tension pressure force. The calculation proceeds with a calculation over all full and surface cells during which velocities are set independent of pressure and the divergence requirement. These velocities assure that vorticity is satisfied at each cell corner. The iteration procedure in the SMAC code then modifies



PRECEDING PAGE BLANK NOT FILMED

ARB An OB cell which has a fluid particle within $\epsilon \cdot DR$ of the arbitrary boundary, where $\epsilon$ is the boundary sensing parameter and is usually set equal to 0.25.

BND A border cell which is neither COR or EXT.

BOR A cell bordering the interior cells. A border cell is not an interior cell and cannot contain fluid.

BOT A COR cell containing a segment of an arbitrary boundary which has its midpoint and angle being stored in the OB cell just below it.

COR A cell which has a line segment of the arbitrary boundary passing through it, however, fluid area to total cell area fraction is less than 0.25. The fluid area is to the left of the line segment. Also, any cell just outside an OB cell is a COR cell.

EMP The cell is empty (contains no fluid particles).

EOC A cell which is either EMP or COR.

EXT Any cell outside a COR cell.

FUL A cell which contains fluid and has no empty neighbor.

LEF A COR cell containing a segment of an arbitrary boundary which has its midpoint and angle being stored in the OB cell just to the left of it.

OB A cell which has a line segment of the arbitrary boundary associated with it (see COR).

OK An ARB cell that does not contain the intersection of a free surface and the boundary.

RIG A COR cell containing a segment of an arbitrary boundary which has its midpoint and angle being stored in the OB cell just to the right of it.

SNC A cell which is also flagged as FUL or SUR and not COR.

SUR A cell which contains fluid and has at least one neighbor with an empty neighbor not COR or EXT.

TOP A COR cell containing a segment of an arbitrary boundary which has its midpoint and angle being stored in the OB cell just above it.

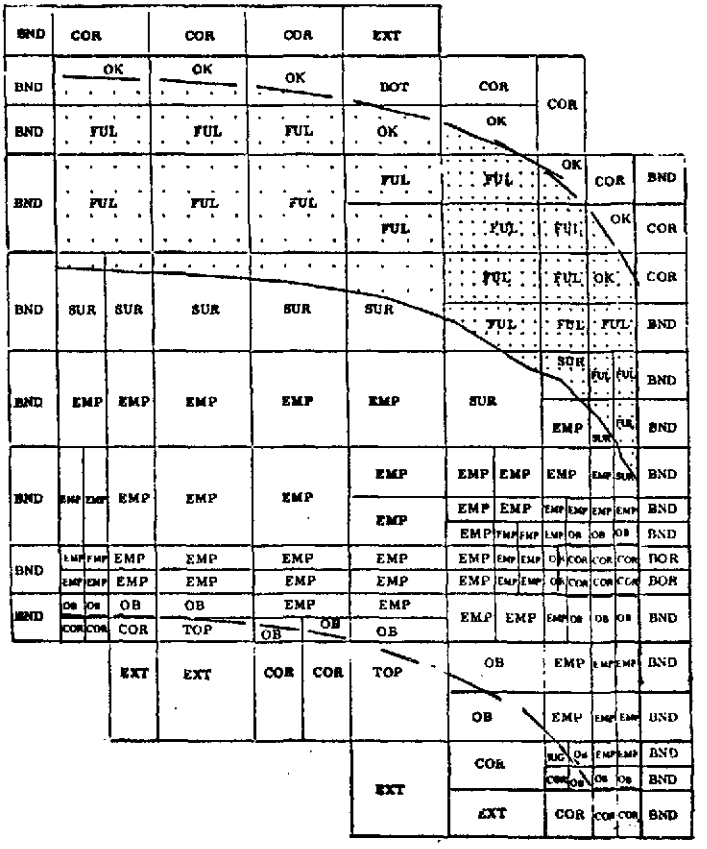

1. All ARB cells are also flagged as ØB.
2. All TØP, BØT, RIG and LEF cells are also flagged as CØR cells.
3. All the above SUR and FUL cells are also flagged SNC.

Figure 1. Variable Grid Network Illustrating Typical Cell Flags



REPRODUCIBILITY OF THE ORIGINAL PAGE IS POOR

these velocities to minimize divergence over all cells by adjusting the pressure in each full cell by an incremental amount. The iteration is complete when a specified convergence criteria is satisfied based on a measure of the pressure change which is proportional to divergence.

When convergence is satisfied, the velocities calculated above are used to move an array of massless particles defining both the surface and the fluid location. It is these marker particles which give the method its name, marker and cell. The surface is defined not only by the above criteria for surface cells but also with an array of surface particles which are moved in a similar manner to marker particles. These surface particles are also used to determine the magnitude of the surface pressure. The graphic output of these particles each time-step and a similar printout of cell-centered velocity vectors are the descriptive output of this method. This is in addition to velocity, pressure, divergence data, and cell flag data which are printed out for each cell.

## 2.1 EQUATIONS OF MOTION

The computer code ERIE solves the Navier-Stokes equations and satisfies the equation of continuity, i.e., divergence for full fluid cells is zero. The basic differential equations are presented below

$$\frac{\partial u}{\partial t} + \frac{1}{r^{\alpha}} \frac{\partial r^{\alpha} u^2}{\partial r} + \frac{\partial uv}{\partial z} = -\frac{\partial \phi}{\partial r} + g_r(t) + \nu \frac{\partial}{\partial z} \left( \frac{\partial u}{\partial z} - \frac{\partial v}{\partial r} \right) \tag{1}$$

$$\frac{\partial v}{\partial t} + \frac{1}{r^{\alpha}} \frac{\partial r^{\alpha} uv}{\partial r} + \frac{\partial v^2}{\partial z} = -\frac{\partial \phi}{\partial z} + g_z(t) - \frac{\nu}{r^{\alpha}} \frac{\partial}{\partial r} \left[ r^{\alpha} \left( \frac{\partial u}{\partial z} - \frac{\partial v}{\partial r} \right) \right] \tag{2}$$

$$D = \frac{1}{r^{\alpha}} \frac{\partial r^{\alpha} u}{\partial r} + \frac{\partial v}{\partial z} = 0 \tag{3}$$

The pressure $\phi$ is normalized with fluid density and has units $L^2T^{-2}$. The above equations are applicable to rectangular coordinates when $\alpha = 0$ and apply to cylindrical coordinates when $\alpha = 1$. The SMAC code utilized ZIP-differencing techniques to solve the above equations using variables identified at specific cell locations. The modification of that code to variable grid, VGSMAC, introduced pecularities to the differencing techniques.

A cell is flagged as a surface (SUR) cell when it contains fluid marker particles and it has at least one adjacent neighboring cell which is flagged empty. On free surfaces the tangential stress condition is

$$\frac{\partial u}{\partial z} + \frac{\partial v}{\partial r} = 0 \tag{4}$$

In addition, the normal stress condition is

$$\phi_N = \phi_N \text{ (applied)} + \frac{2\upsilon}{\delta z} (v_T - v_B) \tag{5}$$

The applied part of the pressure is specified according to the requirement of the problem while the viscous part assures that there is otherwise no net flux of normal momentum through the surface. It is important that the normal stress condition be placed on the free surface rather than at the center of the surface cell.

Tentative velocities are calculated for all full and surface cells without the pressure contribution. These tilde velocities are determined before the final iteration scheme. Then, the pressure in each full cell is modified to minimize the summation of a normalized divergence for all full cells. Thus, tentative velocities are modified by Equations 6 and 7 in the iteration scheme

$$u = \tilde{u} + \delta t \frac{\partial \psi}{\partial r} \tag{6}$$

$$v = \tilde{v} + \delta t \frac{\partial \psi}{\partial z} \tag{7}$$

The viscosity coefficient $\upsilon$ used in Equations 1 and 2 is the sum of a kinematic molecular viscosity and a turbulent viscosity

$$\upsilon = \upsilon_{\text{molecular}} + \upsilon_{\text{turb}} \tag{8}$$

The molecular viscosity is an input quantity and is a fluid property. The turbulent viscosity coefficient is calculated internally in the program as indicated below

$$\upsilon_{\text{turb}} = \text{TURB} \times \ell^2 \max \left( \left| \frac{\partial v}{\partial r} \right|, \left| \frac{\partial u}{\partial z} \right| \right) \tag{9}$$

where

$$\ell = \begin{cases} \text{DR if } \left| \frac{\partial v}{\partial r} \right| > \left| \frac{\partial u}{\partial z} \right| \\ \text{DZ if } \left| \frac{\partial u}{\partial z} \right| > \left| \frac{\partial v}{\partial r} \right| \end{cases}$$

and TURB is an input quality which was held constant at 0.05 (Ref. 3).

This expression for turbulent viscosity is of the form predicted by both Prandtl's mixing-length theory and Taylor's vorticity transport theory. A turbulent viscosity is calculated in a cell containing fluid when at least two of its adjacent neighboring cells also contain fluid. The criteria of requiring fluid in adjacent fluid cells is needed so that $\partial v/\partial r$ and

$\partial u/\partial z$ can be calculated. For the reorientation flow cases examined in this study (Section 3) the magnitude of the local turbulent viscosity coefficient was at least an order of magnitude greater than the molecular viscosity coefficient for most of the problem duration. This indicates that the viscosity coefficient used in Equations 1 and 2 is mainly a result of the turbulent viscosity coefficient.

## 2.2 ERIE COMPUTER CODE

This section describes in detail the calculational cycle in the framework of ERIE. The code ERIE contains a number of features that make it a useful analytical tool for fluid dynamic studies. In particular,

a. The code is written in FORTRAN IV for the CYBER 172 system in overlay structure (Figure 2) and interfaces with the SC-4020 plotter to provide particle and velocity vector plots.

b. The code can be used with either cylindrical or rectangular geometry. Axisymmetric flow can be computed in a cylindrical geometry mode.

c. Grid mesh size may be varied for different areas of the model with a variable grid. The size of the computing mesh can be changed from problem to problem, including both the number and size of cells and the number of particles. The setup allows for different initial conditions and particle resolution in specified regions of the mesh. A scaling feature provides for model and full-scale simulation by changing only one variable.

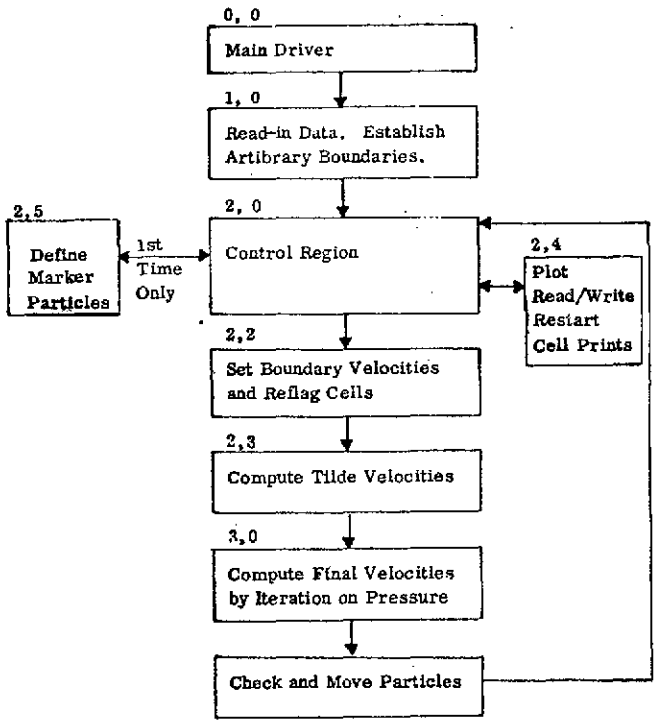


Figure 2. Basic Logic Flow of Overlay for Program ERIE

d. Various boundary conditions are available. Both curved (arbitrary) and straight wall boundaries can be used to represent various shapes.

e. This code can calculate both free-surface and confined flows. Surface conditions may include surface tension forces.

f. Gravitational effects in rectangular coordinates may be included in any orientation

and may be time-dependent. In cylindrical coordinates, only the axial gravity force is appropriate due to symmetry; it may be also time-dependent.

2.2.1 OVERLAY STRUCTURE - Program ERIE makes maximum usage of overlay structure in that the time-consuming pressure iterations are done in a link (3,0) requiring low core storage (Figure 2). The surface tension logic added during this study significantly expanded link (2,2); however that link is not used but a small fraction of the time. The velocity and marker particle plots make this a most descriptive computational tool. The amount of data generated cannot be adequately assessed without reviewing the plots which are generated.

2.2.2 VARIABLE GRID MESH AND CELL FLAGS - The variable grid concept affords a method of analyzing particular sections of the problem in finer detail. Each cell is rectangular as it is in the fixed grid model from which the variable grid program was derived. Each interior cell may have either one or two neighbors in each of the four directions, left, top, right or bottom, i.e., a maximum total of eight neighbors. The primary cell variables in the ERIE code are velocities u and v on right and top sides, respectively; the pseudo-pressure $\psi$ which is cell-centered except for boundary cells where it is located at the segment midpoint; and the velocity divergence, D, which is satisfied for full and surface cells and is the convergence criteria on full cells. The calculation of all these variables is made more complex by the unequal lengths of common cell sides. Special provisions were taken to assure cell variables were interpolated at the correct locations outside the cell being determined. This program computes the above variables throughout a grid mesh in which cells are flagged with one or more flags indicating their fluid state or relation to the boundaries defining the problem. These cell flags were defined in Figure 1 where an example is presented of a variable grid configuration with appropriate cell flags indicated. Only the most significant flag is shown on a cell; a cell may be flagged ØB, ARB, FUL, ØK, and SNC simultaneously.

In addition to the mesh of Eulerian cells, the ERIE code employs a set of massless marker particles which provide a visual representation of the fluid. An essential purpose of these marker particles is to define the position of full and surface cells so that the configuration of the surface can be sensed. Beyond this, the marker particles do not enter into the calculation, but are merely embedded in the fluid and are carried along by it. The particles are inserted at a density per given problem dimension. Since particles primarily impact the flagging procedure, it is often desirable to input denser particle arrays where fluid motion is most rapid or is most interesting. Each cycle the marker particles are moved with an area weighted average of the four nearest u's and of the four nearest v's.

2.2.3 BOUNDARY CONDITIONS - In ERIE both straight line and curved wall boundaries can be used. The ERIE version of the program uses techniques developed by Viecelli for curved-wall arbitrary boundaries (Ref. 7). A series of points are input to specify the curved boundary. These points are a series of coordinates which do not necessarily



REPRODUCIBILITY OF THE
ORIGINAL PAGE IS POOR

lie on the grid-mesh lines. To define the arbitrary boundary segments on the grid mesh, successive points are connected by straight lines and their intersections with the grid mesh are determined. Only one straight line per cell is permitted with intermediate points being dropped.

The following relaxation equation is used to compute the pressure in full arbitrary boundary cells

$$\psi_N^{k+1} = \psi_N^k - \frac{\text{RELAX}}{\lambda} \left[ \left( \vec{V}_M^{n+1} \right)^k \cdot \hat{n} \right]_N \tag{10}$$

In this equation $\hat{n}$ is the normal at the midpoint of the boundary segment associated with cell N and $(\vec{V}_M{}^{n+1})_N^k$ is the liquid velocity at the midpoint of the segment computed with an area-weighted interpolation formula. Clearly $(\vec{V}_M{}^{n+1})_N^k$ is one of the iterates and must be recomputed each time the pressures and velocities are adjusted. The relaxation parameter and minimum mesh dimension are RELAX and $\lambda$, respectively. Note that pressure is not adjusted to satisfy divergence or net flux out of the cell but is adjusted proportional to the velocity directed perpendicular to the normal vector at the segment midpoint. If liquid is flowing across the boundary the pressure is increased until the outflow stops. If liquid is tending to separate from the boundary the pressure is decreased until the liquid flows tangent to the boundary.

Where free surfaces intersect curved wall boundaries, special procedures are required. The pressure at the intersection point should equal the ambient pressure. However the pressure is defined only on the Eulerian net and it is sometimes not possible to zero the flux at the boundary consistent with vanishing divergence without introducing a pressure. In most circumstances the liquid in the cell will be part of a much larger mass. When there are one or two liquid neighbors, the velocity components at the sides in contact with the liquid are preserved, and those at the open and boundary sides adjusted to make the velocity tangent at the boundary consistent with vanishing divergence. In the case of one liquid neighbor, the velocities at the opposite cell sides are assumed equal, and the component with both sides open or boundary is adjusted. If the velocity at the boundary is initially directed away from the boundary, nothing need be done. The remaining possibility is that there are no liquid neighbors, as happens when a small isolated element strikes the boundary. In this case we set the component of the particle velocity normal to the boundary equal to zero and preserve the tangential component. If a gravitational force is present we accelerate the particle velocities by the component of the gravitational vector tangent to the boundary. This is a free slip condition.

2.2.4 TIME-STEP - The procedure for calculation of maximum time-step uses two stability and two accuracy criteria. The length dimensions (DRSTEP, DZSTEP) are selected equal to the average of the cell mesh sizes, which may exceed the accuracy criteria of the smallest cells. Therefore, care must be taken in selecting these variables which determine the maximum allowable time-step. The calculated time-step is used except

that when a print interval time is exceeded, the time-step is dropped to the print time. To avoid an extremely small step in this latter case, the criteria is relaxed so that a step to a print cycle may exceed the calculated time-step by forty percent.

The first stability criteria exists to satisfy conditions imposed by the differencing technique

$$\delta t \leq \frac{(\mathrm{DRSTEP})^2 \, (\mathrm{DZSTEP})^2}{4 \upsilon \left[(\mathrm{DRSTEP})^2 + (\mathrm{DZSTEP})^2\right]} \tag{11}$$

The second stability criteria exists to satisfy "Courant" condition and uses the wave speed and fluid depth

$$\delta t \leq \frac{2 * \mathrm{DRSTEP} * \mathrm{DZSTEP}}{(\mathrm{DRSTEP} + \mathrm{DZSTEP})\, c} \tag{12}$$

where c is the wave speed. This stability criteria was not a limiting value during this study. With active surface tension, $c = \sqrt{gh + 2\pi\beta/3 \cdot \mathrm{DRSTEP}}$.

The third and fourth restrictions are related to accuracy so that a particle does not move across an entire cell in a time-step. These accuracy criteria were the limiting criteria during this study

$$\delta t \leq \frac{\mathrm{DRSTEP}}{2u_{max}} \tag{13}$$

$$\delta t \leq \frac{\mathrm{DZSTEP}}{2v_{max}} \tag{14}$$

To insure that particles do not move across an arbitrary boundary during a time step, the particle sensing parameters are included

$$\delta t \leq \mathrm{DRSTEP} \times 2 \times \epsilon / u_{max} \tag{15}$$

$$\delta t \leq \mathrm{DZSTEP} \times 2 \times \epsilon / v_{max} \tag{16}$$

where $\epsilon$ is the boundary sensing parameter. This latter criteria is only used when the fluid is going toward the boundary (not parallel to or away from the boundary).

2.2.5 CONVERGENCE CRITERIA - To reach an acceptable solution, the iteration scheme continues to adjust the pressure throughout the fluid, i.e., the FUL and OK cells, until the convergence criteria have been satisfied. Recall the tilde (temporary) velocities are adjusted by the pressure gradient to obtain the final velocity distribution which is tested for divergence. Convergence criteria are tested against the sum of the



REPRODUCIBILITY OF THE
ORIGINAL PAGE IS POOR

normalized divergence over all cells rather than the divergence of a single cell which would be a more stringent requirement. The tilde velocities are modified into final velocities for the cycle in a way that will preserve the vorticities that have been correctly implanted into the fluid. In the case of non-OK cells this will now bring the divergence to zero, while in the case of OK cells it will cause the fluid to flow parallel to the arbitrary boundary. A delta pressure is determined for each FUL and OK cell for each iteration. New velocities are then computed for that cell as a function of the newly defined pressure before proceding to the next cell. When all cells have been treated in this fashion, a test is made to see if this pressure field resulted in convergence. If not, the procedure is repeated for another iteration.

At each iteration, k, the change in pressure for FUL and OK cells is a function of the quantity D (D ≡ divergence for FUL cells) which is computed for all FUL and OK cells according to the following expressions.

D Calculation for FUL Cells:

$$D_N^{k+1} = \frac{1}{r_N \delta r_N}\left[RIP_N u_N^k - RIP_{NL} u_{NL}^{k+1}\right] + \frac{1}{\delta z_N}\left[v_N^k - v_{NB}^{k+1}\right] \tag{17}$$

where $RIP_N$ and $RIP_{NL}$ are radial distances to cell edges.

D Calculation for ØK Cells:

$$D_N^{k+1} = \frac{DN\emptyset RX_N * UK_N + DN\emptyset RY_N * VK_N}{MAX\,(\delta r_N, \delta z_N)} \tag{18}$$

where $UK_N$ and $VK_N$ are the u and v components of the velocity at the midpoint of the boundary segment associated with cell N.

The pressure iteration proceeds through the cells in the order in which they were input. Only one matrix is used for $\psi$, so that the program uses the latest values (iteration number k+1) for velocities whose index is smaller than that of cell N and old values (iteration number k) for those velocities whose index is greater than N.

The pressure of cell N at the end of k+1 iterations is then defined by

$$\psi_N^{k+1} = \psi_N^k - \xi_N D_N^{k+1} \tag{19}$$

where $\xi_N$ is a relaxation parameter defined by

$$\xi_N = \frac{ALP\,\{[MIN\,(\delta r_N, \delta z_N)]^2\}}{\delta t} \tag{20}$$

where ALP is an input variable. The convergence test is

$$\left[\frac{\sum_{N=1,NCELL} TEMP^2}{\sum_{N=1,NCELL} (\psi_N - TEMP)^2}\right]^{1/2} < EPS \qquad (21)$$

where TEMP = $\xi \times D_N$ for FUL cells has been satisfied for all FUL cells. Here EPS is usually on the order of $8 \times 10^{-4} \times$ MIN ($\delta r_N^{1/2}$, $\delta z_N^{1/2}$), (Ref. 7).

On the relaxation of the gravitational field in impulsive-g settling, convergence problems were encountered. The pressure field is the key variable in convergence; a field which ranged from 0 to 1000 was decreased to the order of 0 to 10 when the liquid head was removed. Several convergence techniques were attempted to reduce the number of iterations. One scheme involved convergence of single cells rather than overall convergence. Another scheme involved a sophisticated technique encompassing a steepest ascent gradient method. The latter proved to be less efficient in this situation than the current approach.

To reduce the iterations, an approach valid in the solution of certain classes of simultaneous equations was employed. Three consecutive iterations are used to establish a trend for extrapolation of each pressure value to a new value. The equations used are

$$P_i^{new} = P_i^{(k-1)} + \frac{P_i^{(k)} - P_i^{(k-1)}}{1-\mu} \qquad (22)$$

in which $\mu$ is defined by

$$\mu = \sum_{i=1}^{N} \left| \left[ \frac{P_i^{(k+1)} - P_i^{(k)}}{P_i^{(k)} - P_i^{(k-1)}} \right] \right| \Big/ N \qquad (23)$$

In the preceding equations, the superscripts k-1, k, and k+1 identify the three previous iterations, k+1 being the most recent. The variable $\mu$ is constrained to be $\leqq 0.99$ to prevent overextrapolation.

Currently this procedure is not activated until 60 iterations have passed. It is necessary to wait a sizeable number of iterations to assure that transients have disappeared and convergence is underway. Additionally, extrapolation is repeated every 40 iterations after the initial 60 if required. The above technique has been checked out on the impulsive-g model case and in all instances convergence was attained. This

procedure resulted in improved convergence in comparisons made with and without it. In no case were the results slower. It was made a permanent part of the program and used in all four cases of this study. Frequently, convergence was reached in less than sixty iterations on Cases 2 and 3. For Case 4, a typical number of iterations was 12, the minimum permitted for this case. It has been recognized that less than 12 iterations may lead to false solutions.

2.2.6 SURFACE TENSION FORCE - A major task in this study was the improvement in the surface tension logic used in computer code ERIE. In investigating fluid dynamic behavior at reduced gravity, the surface tension forces become important at Bond numbers below 10. Below Bond numbers of 1, surface tension forces dominate acceleration forces. Since fluid behavior during the coast phase of the Centaur vehicle is of interest when Bond numbers are 10 and below, it is necessary to consider surface tension forces.

In this study a method suggested by Daly (Reference 8, 9) was used for adding surface tension forces to the marker-and-cell code. The surface tension force is applied as a pressure across the interface acting at the intersection of the interface with lines through surface cell centers. In the following paragraphs, various details of the logic will be discussed.

The surface tension pressure is defined by the equation

$$\psi_{ST} = \beta\,(1/R_1 + 1/R_2) \tag{24}$$

where $\beta$ is a kinematic surface tension coefficient ($L^3/T^2$) and $R_1$ is a radius of curvature in the two dimensional plane of the paper (a transverse force) and $R_2$ is a radius of curvature (a circumferential force) in a plane perpendicular to the former plane and passing through the interface point perpendicular to the tangent to the curve in plane one. In plane coordinate systems, $R_2$ is not considered.

This method makes use of the surface marker particles which define the surface location. These are moved each time step with the velocities which have been determined for each full or surface cell. After movement of the particles, the pressure field along the interface is determined from the curvature of the interface defined by these particles. Particles are checked for overall spacing to assure that movement has not resulted in large gaps or particles moving too close to one another. If this occurs, particles are added or deleted as the situation requires.

The next step in the process is the relocation of the end points of the surface line. These points will have been moved earlier with the local velocities. Since no-slip boundaries are used, the particles will move parallel with the straightline boundary

with the velocity of the adjacent cell. For arbitrary boundaries, a similar parallel flow is assured. However, the location of each end boundary point is still relocated each step to satisfy contact angles which are input as a specification: contact angle = $const_1 + const_2\ (time)^{const_3}$ for each end. Boundaries are input as a series of points defining straight lines; as few as two may be input to define a line for intersection of each end of the interface. Although zero contact angle fluids may be used, the macroscopic angle from the center of the adjacent cell is larger and this is the angle which is required. The proximity to the boundary of the second and second to last surface marker particle is limited by an input specification of a perpendicular distance to the wall, (Figure 3). If the particle is closer than this distance, the particle is deleted and the next particle is tested until one is found which satisfies this minimum distance requirement. The contact angle is computed between this point and the appropriate boundary segment and a point defined on this boundary segment which satisfies the angle requirement. Special logic was required for convex boundaries since perpendiculars and some specified contact angles are not always defined. In these cases, the nearest point on the boundary is located and used to satisfy the boundary point for that time step.

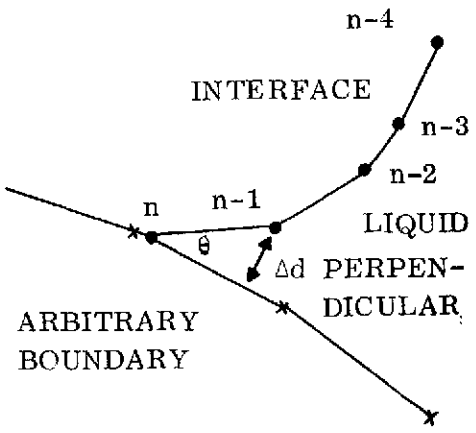


Figure 3. Contact Angle Definition From Interface Particle (n-1) to Particle (n)

After the points have been defined, they are divided into x and y sequences, since spline fits require monotonicity. Spline fits also require five points in the sequence. Therefore, if five sequential points fail to satisfy the monotonicity test, smoothing is applied. If no improvement occurs, a circular arc fit is used. The sequence switches from r to z when the slope of five consecutive segments exceeds 1.5 or from z to r when the slope is less than 0.666 for five consecutive particles

$$\left| \frac{z_{i+1} - z_i}{r_{i+1} - r_i} \right| > 1.5, \qquad i = k,\ k+1,\ k+2,\ k+3,\ k+4, \tag{25}$$

and

$$\left| \frac{z_k - z_{k-1}}{r_k - r_{k-1}} \right| < 1.5 \tag{26}$$

A sequence of points with a tight radius of curvature are also smoothed to avoid unrealistic pressures due to local deviations. The spline fit, which uses five points, also requires monotonicity of two points into the next sequence, with program stops resulting if this is not satisfied. An exchange of two surface particles sometimes satisfied this requirement.

After the sequences are defined, the sequences are solved as a series of cubics with a spline fit interpolation scheme. It is the coefficients of the matrices which result that are used to define first and second derivatives at the r, z locations of the intersection of the interface segments and lines through surface cell centers. The radius of curvature are defined by the following equations for the radial sequence

$$R_1 = [(z')^2 + 1]^{3/2} / z'' \tag{27}$$

$$R_2 = r[(z')^2 + 1]^{1/2} / |z'| \tag{28}$$

and for the axial sequence

$$R_1 = [(r')^2 + 1]^{3/2} / r'' \tag{29}$$

$$R_2 = r[(z')^2 + 1]^{1/2} / |r'| \tag{30}$$

With the radius of curvature defined, the equation for surface tension pressure is solved. In the Marker-and-Cell technique, pressures are always defined at cell centers with the exception of arbitrary boundary cells. Thus the pressure must be translated to the center of the surface cell based on the following equation, as was illustrated by Figure 4 taken from Reference 10

$$\psi_N = (1 - \eta)\,\psi_F + (\psi_{ST} + \psi_{NS})\,\eta \tag{31}$$

in which

$\psi_N$ = the pressure at the center of the SUR cell

$\psi_F$ = the adjacent FUL cell pressure (e.g. point C in Figure 4)

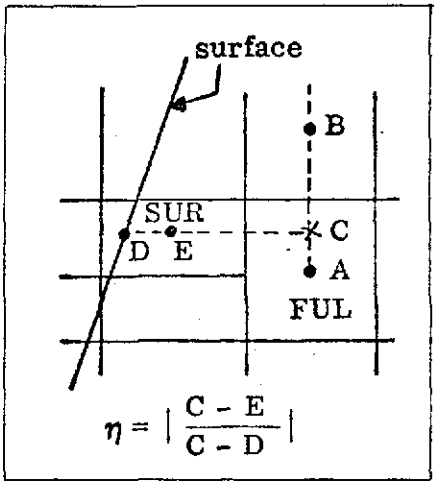


Figure 4. Surface Tension Pressure Solution

$\psi_{ST}$ = surface tension pressure at the closest intersection point as described above

$\psi_{NS}$ = normal stress pressure

$$\eta = \left| \frac{D_{\text{full cell-surface cell}}}{D_{\text{full cell-surface intersection}}} \right|$$

The value of $\eta$ is confined to $0.667 \leq \eta \leq 2.0$ to insure that only pressures from nearly full cells are used. Equation 31 is used so that when the regular formulas are used for computing velocities in FUL cells adjacent to SUR cells, the desired pressure is simulated at the surface rather than at the center of the SUR cell.

2.2.7 SURFACE TENSION VERIFICATION - A series of runs were made to verify the surface tension logic. A circular interface was input and the radius of curvature was evaluated at the intersections of cell centers to verify the calculation results. A similar input was made for a sine curve so that the known values could be compared with the program calculated values. The two surface shapes indicated appropriate values were being calculated for the surface tension pressure.

A typical settling fluid configuration was input to evaluate the method of wall contact angle simulation for both straight line and curved boundaries. The fluid was placed forward in the tank to simulate conditions prior to settling for engine restart. The fluid is initially in contact with the cylindrical wall and later with the tank aft bulkhead. Results of this simulation are shown in Figure 5. This particular sequence is shown to indicate the transfer of the end point data from one boundary to the other. Until 0.2435 seconds, the interface remained attached to the vertical straight line boundary (cylinder wall) because the end point data only included two points on that line. In a problem restart, interface end point boundary information for the arbitrary boundary (bottom bulkhead) was input. The interface then transferred automatically from the side to the bottom boundary and the problem continued smoothly.

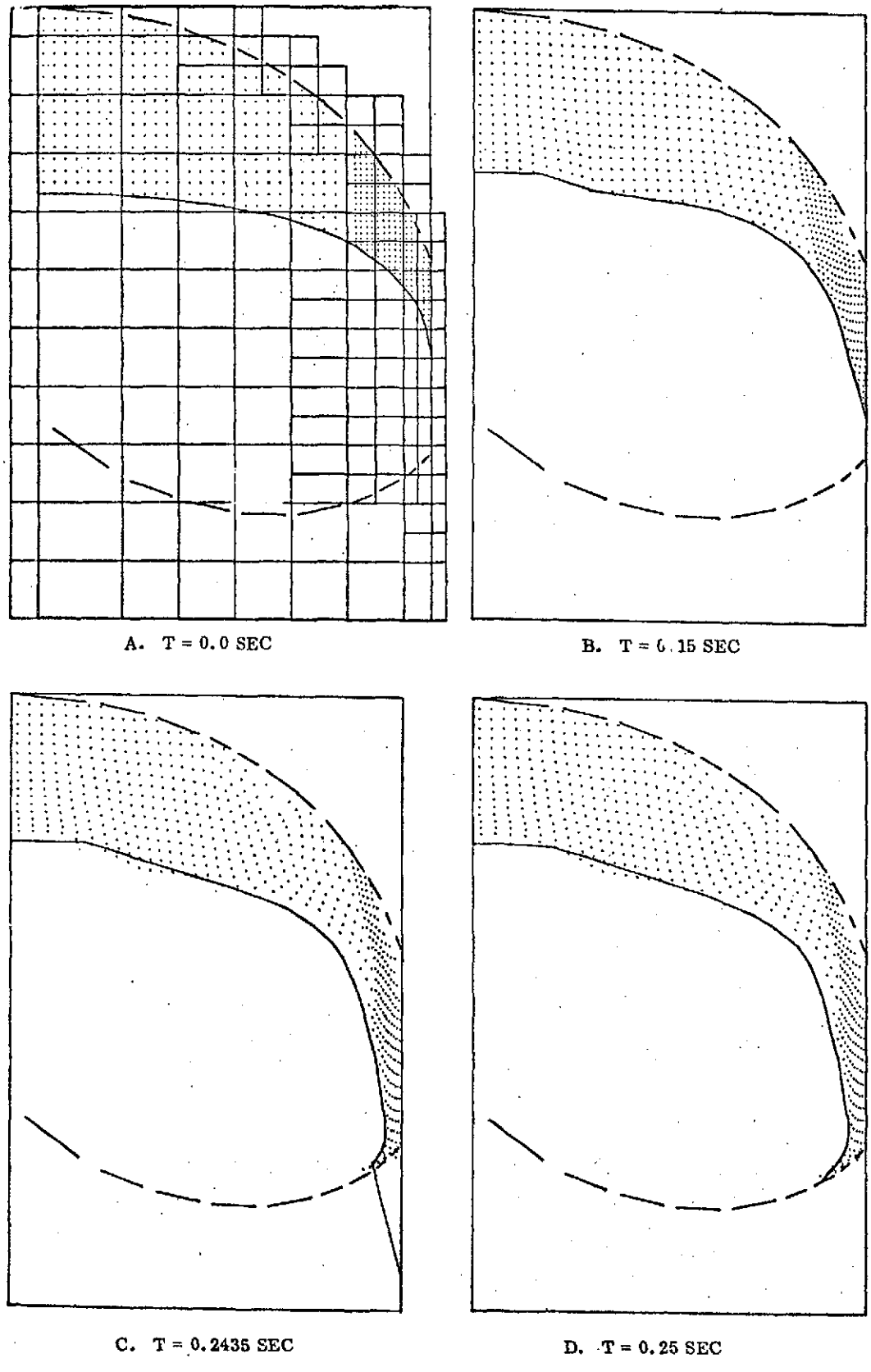


Figure 5. Test Case for Verification of Surface Tension and Contact Angle Logic

# 3

## FLUID DYNAMIC SIMULATIONS

The marker-and-cell program ERIE with modifications for surface tension (Section 2.2.6) was used for the simulation of both model and full-scale fluid motion. A total of four cases were considered, two model settling cases modeling the Centaur fuel and oxidizer tanks, a full-scale settling case for the Centaur oxidizer tank, and a mixing simulation in a full-scale Centaur fuel tank. The former two cases duplicated similar investigations in drop tower tests at the NASA Lewis Research Center. The fuel tank model case was unique in that the potential for impulsive settling was investigated. Details of these cases are summarized in Table I.

TABLE I. FLUID AND PROPERTY DATA FOR FOUR MODEL CASES

| | Radius cm | Fluid | % Liquid | Bond Number Initial | Acceleration cm/sec$^2$ | $\nu$ cm$^2$/sec | $\beta$ cm$^3$/sec$^2$ |
|---|---|---|---|---|---|---|---|
| Case 1 | 5.5 | Ethanol | 65 | 15 | -73.5[1] | 0.01520 | 28.3 |
| Case 2 | 7.5 | FC-78[2] | 25 | 10 | -60.8 | 0.00477 | 7.67 |
| Case 3 | 152.4 | $LO_2$ | 9 | 15 | -1.10 | 0.00167 | 11.7 |
| Case 4 | 152.4 | $LH_2$ | 65 | 100 | +0.116 | 0.00192 | 27.0 |

Note 1. Acceleration set to +0.001 cm/sec$^2$ at 0.30 sec after impulsive settling.
Note 2. A fluorocarbon solvent registered by Minnesota Mining Mfg. Co.

The initial fluid velocities for all cases were zero. The interface configuration was defined by the initial Bond number stated in Table I with the exception of Case 4 where a flat interface was selected. Interface shapes for cylinders were determined from the data by Hastings (Ref. 11) and the interface shapes in the oxidizer tank were from Concus (Ref. 12) who presents data for ellipsoids. The settling accelerations resulted in Bond numbers of 80, 450, and 1800 for Cases 1 through 3, respectively. For Case 4, the initial Bond number of 100 was held constant for the duration of the run.

Other problem specifications common to all cases included free-slip boundaries and a turbulent viscosity coefficient of 0.05 (Ref. 3). All cases were modeled with only the right half of the tank represented, assuming symmetry about the centerline; the problems were run with the cylindrical coordinate option. Although the Centaur fuel tank has baffles, neither fuel tank simulation here considered baffles. The drop tower model did not use baffles. Baffles are within the capability of marker-and-cell techniques and were considered in Reference 1. In going from a model to a full-scale tank, the



PRECEDING PAGE BLANK NOT FILMED

same cell configuration can be used and the change in dimensions covered by a scaling factor. This was done for both full-scale cases where tanks of 7.0 and 6.696 cm were scaled by factors of 21.7714 and 22.7584, respectively. A scaling factor was also used to reduce Case 1 from 7.0 to 5.5 cm. The number of cells and particles used will be discussed with the individual cases.

### 3.1 IMPULSIVE-G SETTLING - MODEL CASE 1

Impulsive settling consists of applying thrust to the vehicle for a brief period of time to set the fluid in motion, then stepping down or ceasing thrust until such time as the fluid is nearly collected. When that occurs, settling thrust is again applied prior to engine start or engine start may occur with no further settling thrust. The NASA Lewis Research Center performed a drop tower test to demonstrate the potential for this approach to propellant settling. The results of their test are illustrated schematically in Figure 6 where the interface shape is shown at various times during the drop. Note that the liquid has not reached the bottom bulkhead when thrust ceases at 0.30 sec, yet the fluid continues to collect until approximately 3 seconds. Beyond this period the fluid returns to a static interface configuration.

It was the object of this study to model the above described behavior with the ERIE code. Surface tension effects dominate in this problem after the thrust is terminated, presenting a valid test of surface tension forces. A Centaur model fuel tank of the dimensions used in the drop tower test, similarly without baffles, was selected (Figure 7). The configuration utilized 400 cells with an initial array of 2272 particles. Final particle array was 2728 particles. The flow initially moved down the side wall at a rate similar to the drop tower test. Marker particle and velocity vector plots are shown in Figures 8 and 9. The grid configuration is shown in Figure 9A. This was the first simulation with surface tension active. A contact angle of 20° from the center of the cell nearest to the wall was selected to represent this wall phenomena. This was derived from a consideration of the macroscopic angle which results for settling Bond numbers with zero contact angle fluids.

Flow simulation went smoothly down the sidewall, the flow reaching the corner at 0.5 seconds, not appreciably different from model results. A filling-in occurred in the corner area and flow simulation continued to follow the model at 0.86 seconds elapsed. Velocities in a radial direction along the bulkhead were weaker than anticipated from this time onward. After 0.9 seconds, velocities in the lower corner region took on an eddy motion and curled back over the top to fill in fluid in this region rather than proceeding across the bulkhead. This phenomenon continued for nearly one-half second and is not explainable. During this period the simulation falls behind the drop tower model. At approximately 1.5 seconds the flow again continued toward the centerline. The simulation was terminated at 1.91 seconds when flow had nearly reached the centerline.

One measure of the progress of this simulation was a slowing down of velocities along the wall due to turbulent dissipation. This phenomena started at 0.3 sec when thrust

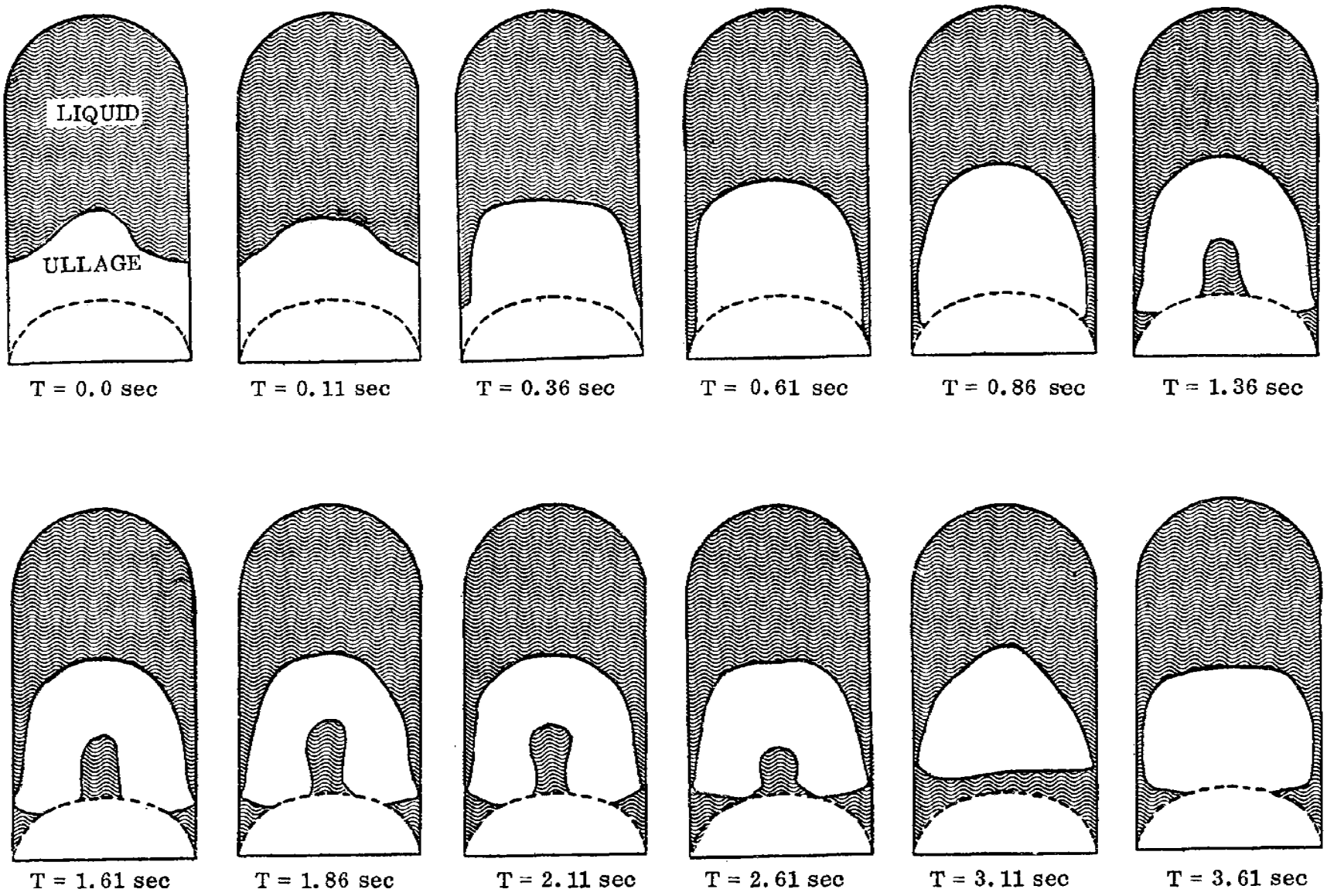


Figure 6. Drop Tower Results for Impulsive-Settling With Model Centaur $LH_2$ Tank - Case 1 - 0.30 Seconds Thrusters On

REPRODUCIBILITY OF THE ORIGINAL PAGE IS POOR

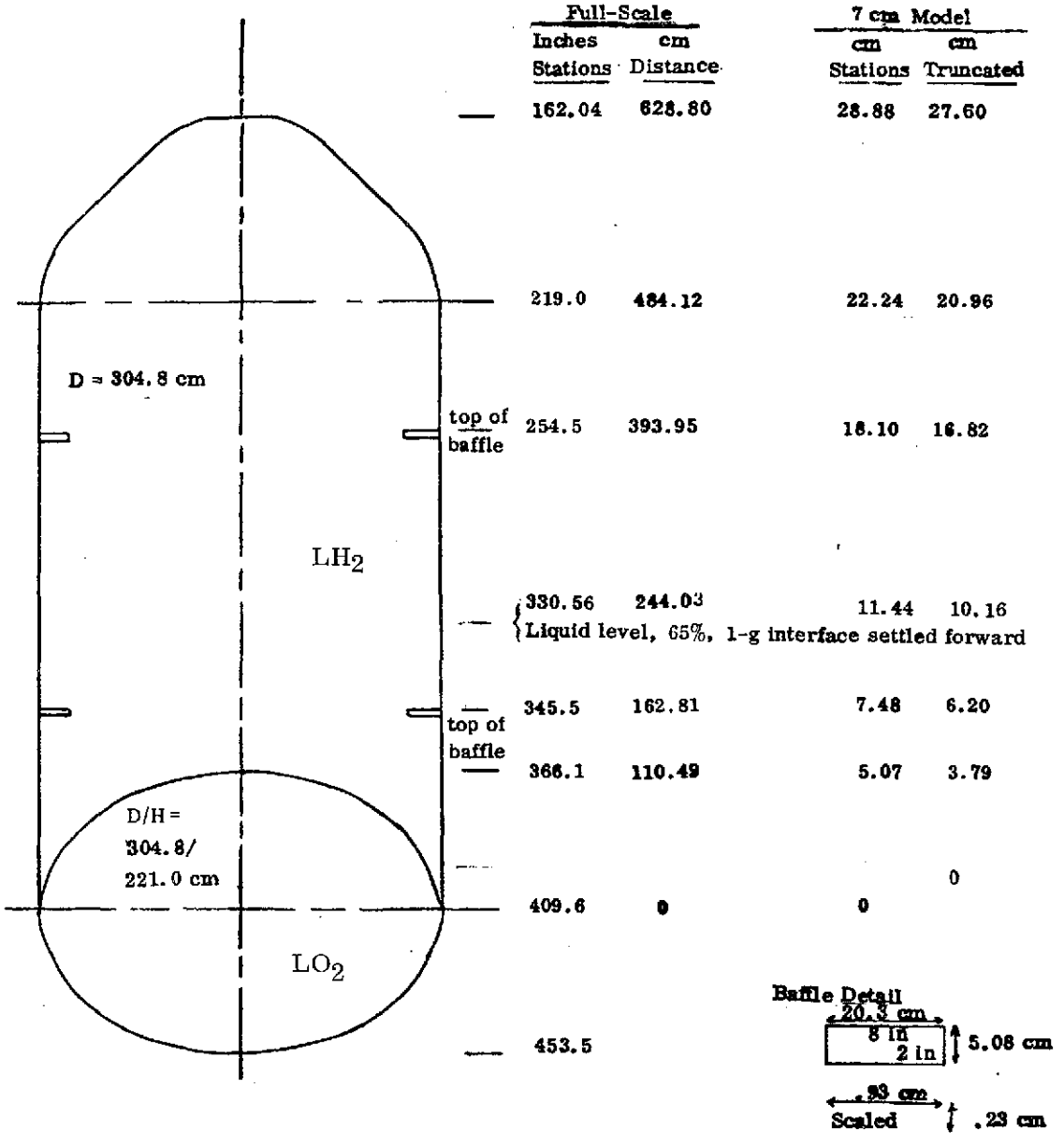


Figure 7. D-1T Tank Configurations With Full-Scale and Model Dimensions

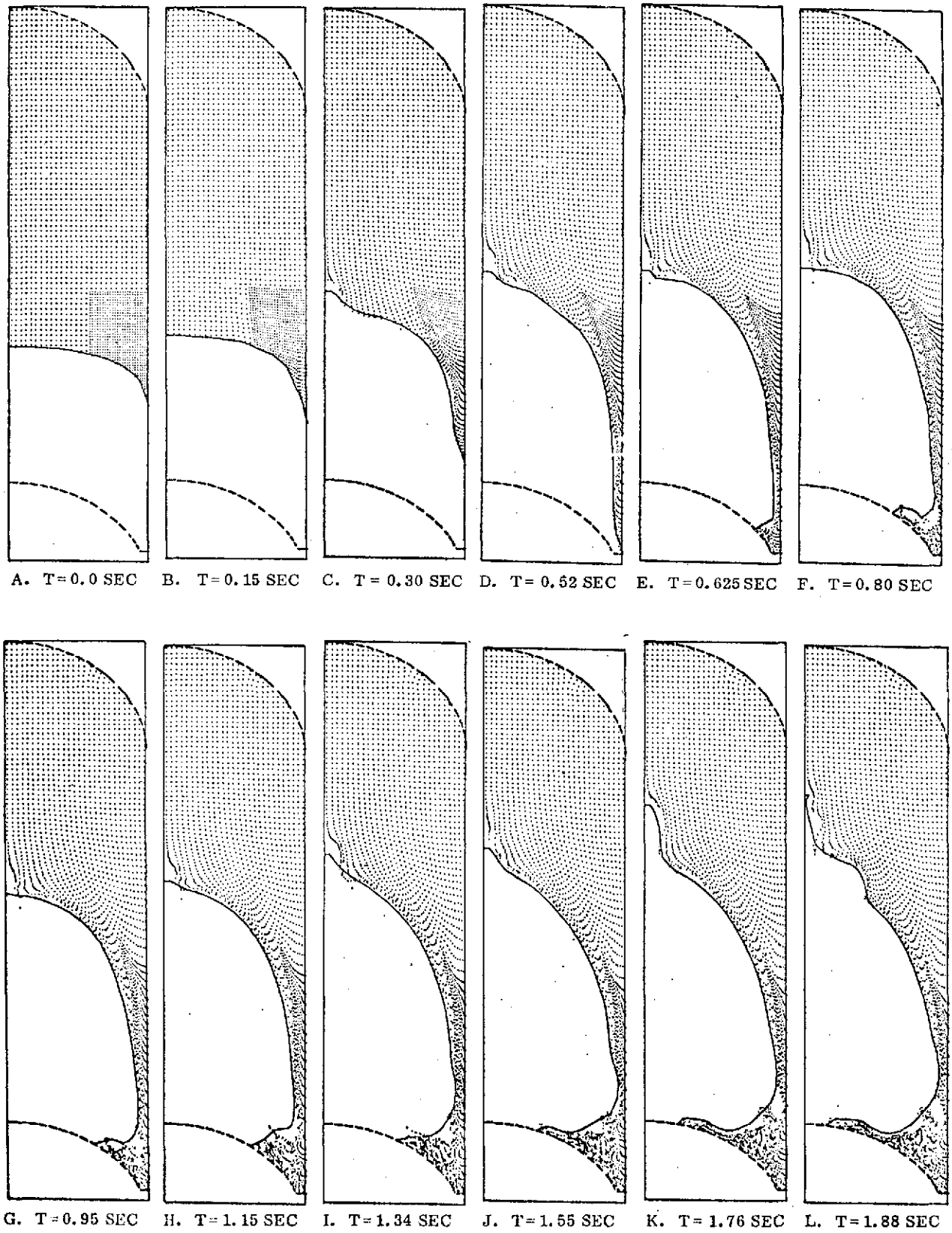


Figure 8. Marker Particle Plots for Model Simulation of Impulsive-G Settling, Case 1

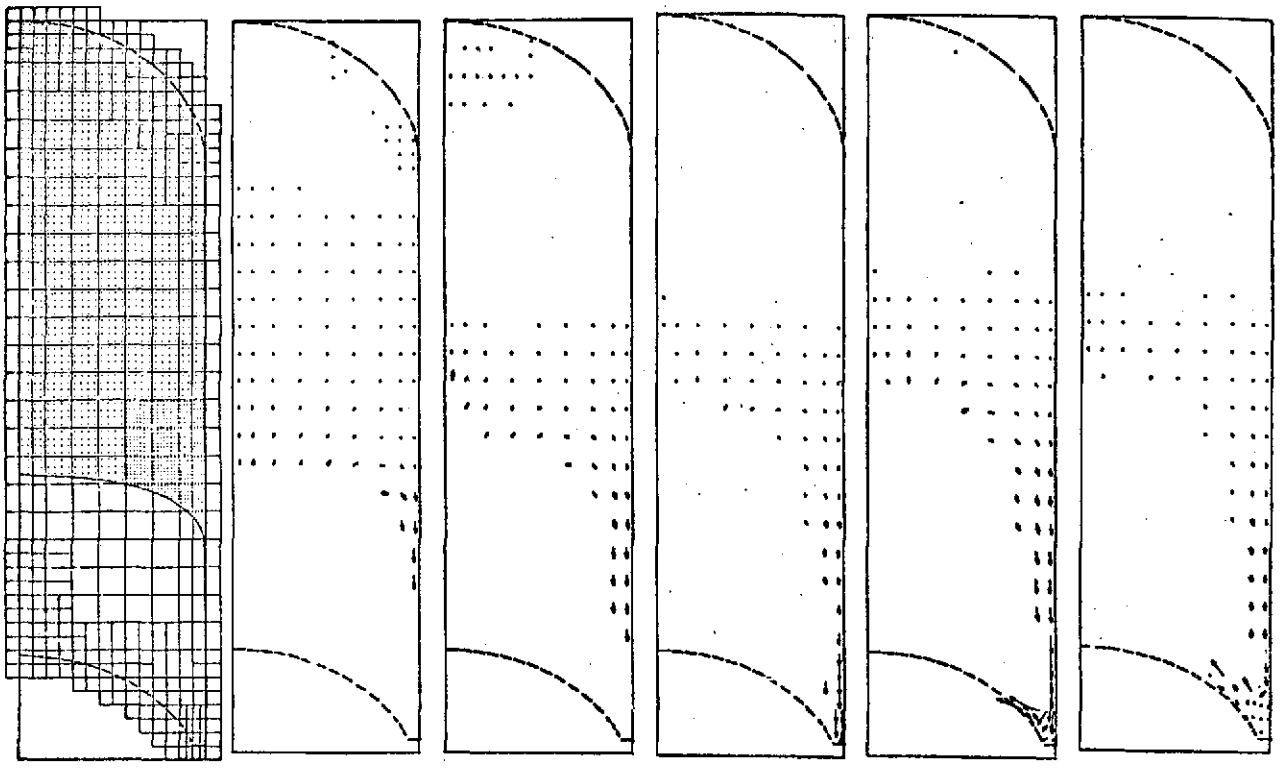

A. T = 0.0 SEC B. T = 0.15 SEC C. T = 0.30 SEC D. T = 0.52 SEC E. T = 0.625 SEC F. T = 0.80 SEC

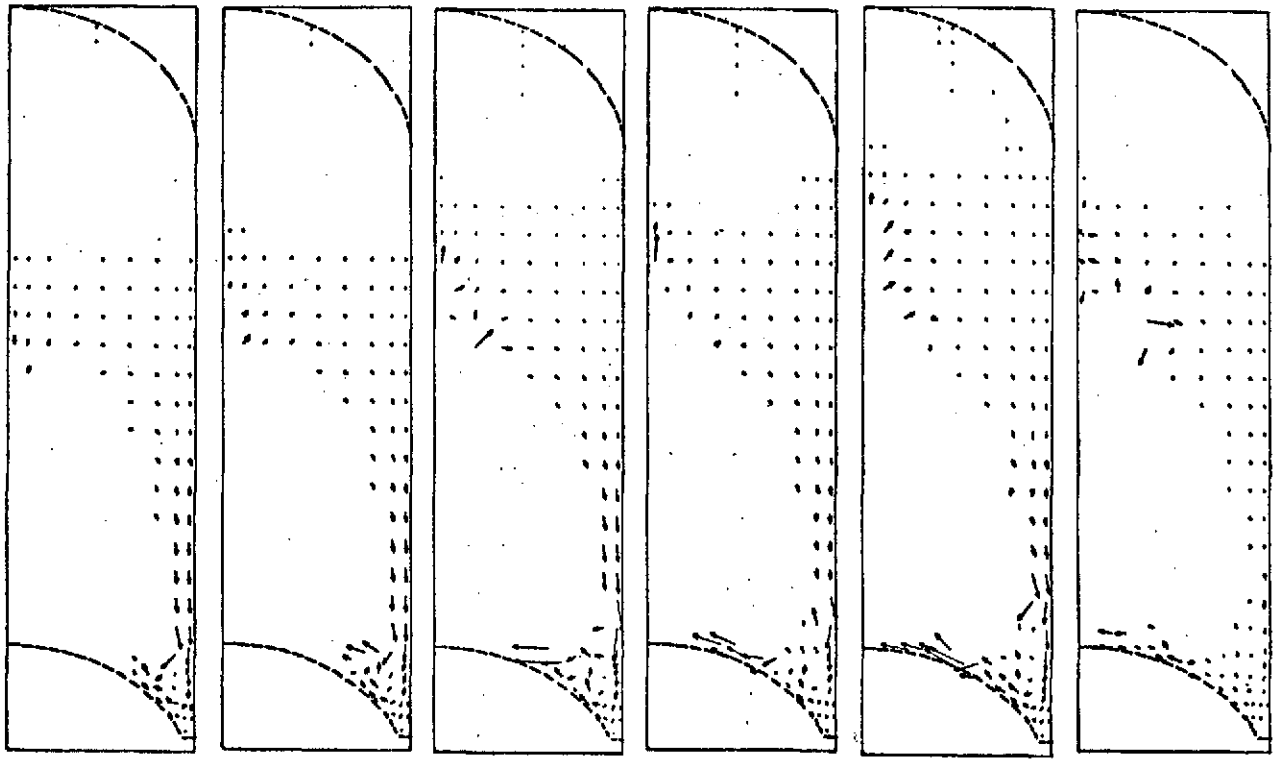

G. T = 0.95 SEC H. T = 1.15 SEC I. T = 1.34 SEC J. T = 1.55 SEC K. T = 1.76 SEC L. T = 1.88 SEC

Figure 9. Velocity Vector Plots for Model Simulation of Impulsive-g Settling, Case 1



REPRODUCIBILITY OF THE
ORIGINAL PAGE IS POOR

terminated and was tracked for several sidewall cells where the thin film existed for the duration of the run. The results are shown in Figure 10 where velocities down the wall are plotted versus simulation time; cell distances above the bottom corner are identified. It was anticipated the problem could be continued until such time as surface tension effects caused the flow pattern to stagnate and reverse to an upward direction as occurred in the drop tower model (Figure 6). The flow stagnation described above and convergence problems prevented the evaluation of this behavior.

Difficulties with convergence were encountered during much of this run beyond 0.30 seconds. This problem was discussed in Section 2 where a temporary solution to this difficulty was presented.

## 3.2 CENTAUR $LO_2$ TANK SETTLING - MODEL CASE 2

This simulation was a settling study of the Centaur oxidizer tank. It was a case patterned after drop tower work by the NASA Lewis Research Center. The Centaur full-scale oxidizer tank is shown in Figure 11. The thrust barrel was a major item in establishing this model. The basic structure and openings in the full-scale thrust barrel are shown in Figure 12C. In this 1/20 scale drop tower modeling, the holes were simulated

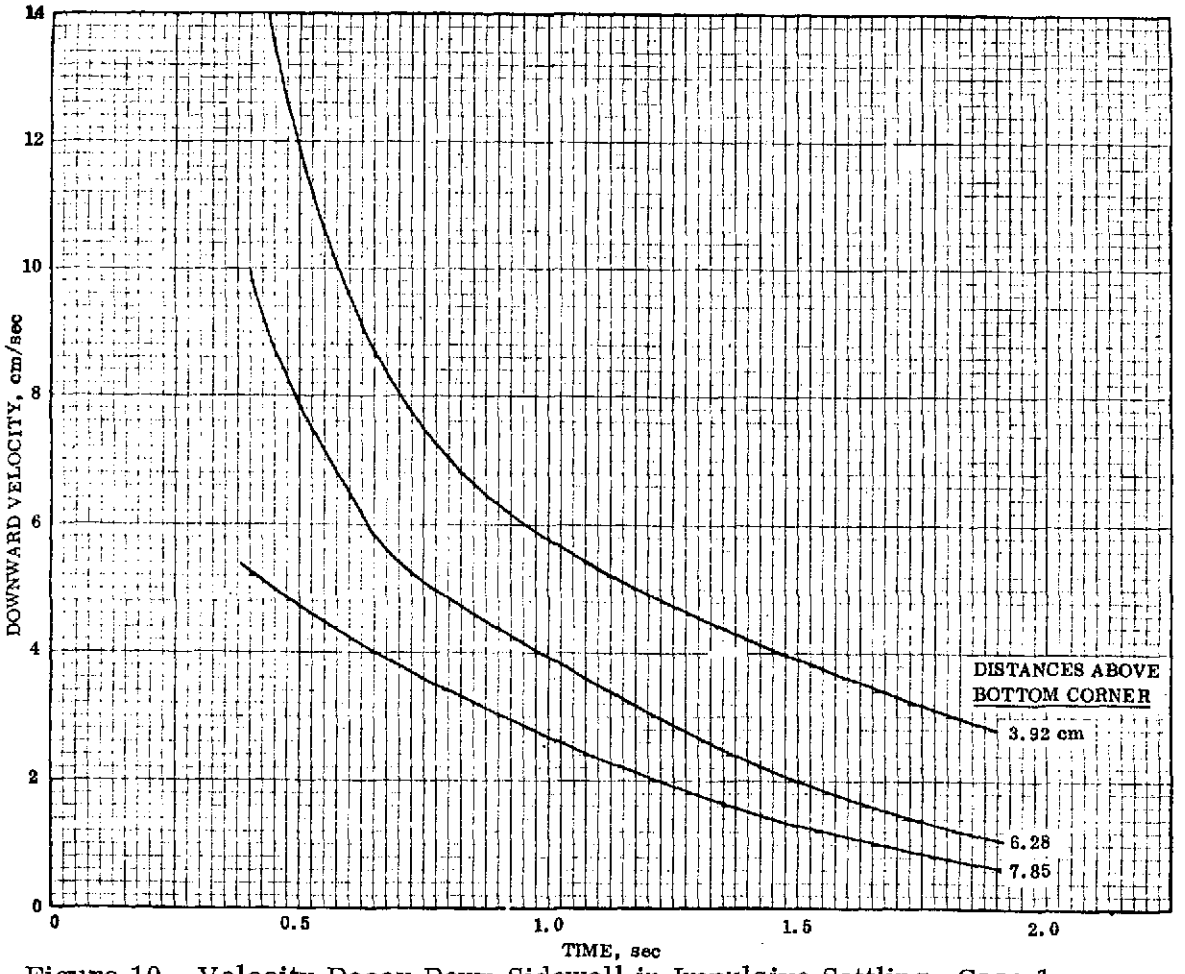


Figure 10. Velocity Decay Down Sidewall in Impulsive Settling, Case 1

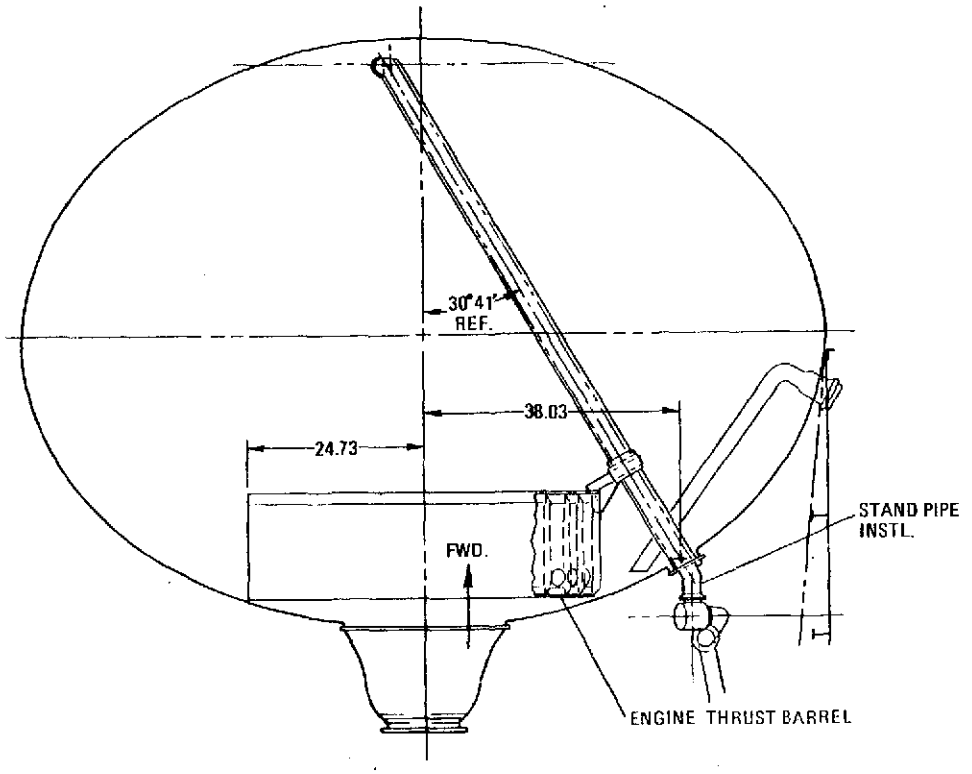


Figure 11. Configuration of Centaur D-1T $LO_2$ Tank Including Thrust Barrel

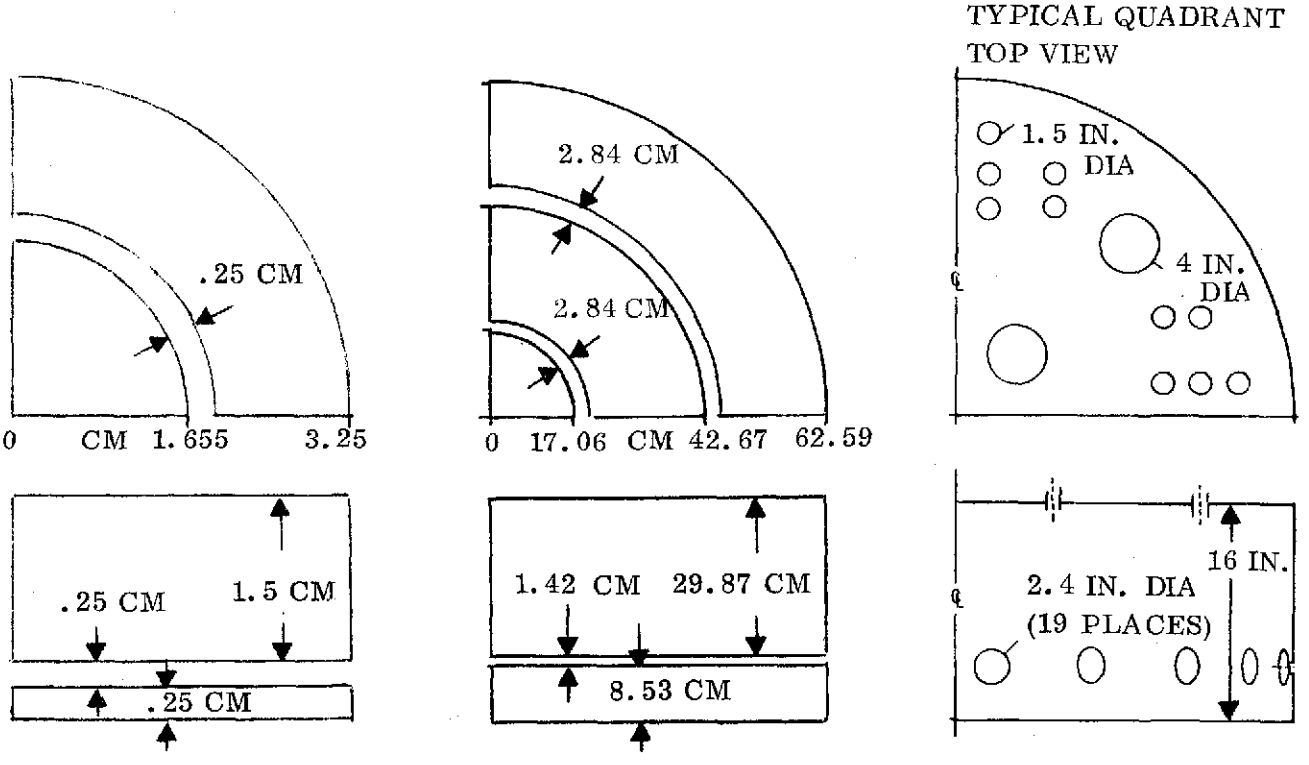


A. Model Simulation Dimensions - Case 2

B. Full-Scale Simulation Dimensions - Case 3

C. Full-Scale Dimensions

Figure 12. Centaur D-1T $LO_2$ Tank Thrust Barrel and Cover Details

with only two slits which, in reality, are annuli in a three-dimensional model due to axial symmetry. A top slit represents 8 of the 0.5 cm dia holes while a side slip represents 20 of the 0.3 cm dia holes. In the model, the tank radius is 7.5 cm and the height 11.0 cm; the eccentricity of the tank is 0.68. The radius of the thrust barrel, Figure 12A, is 3.25 cm, the height is 2.0 cm. The side holes are represented with a 0.25 cm slit and the upper holes with a 0.25 cm slit.

The tank was modeled with 239 cells with 812 particles indicating the 25 percent liquid residual. Two densities of particle spacing were used in an effort to preclude cells voiding of particles in the leading edge flow. The densities were 36 and 100 per square cm. The interface shape for a tank with $\epsilon = 0.68$, Bo = 10, and a fill of 25 percent was taken from Concus where the interface shape is graphically presented (Ref. 12).

Marker particle plots for this case appear in Figure 13 and the vector plots in Figure 14. The grid for this model tank is shown in Figure 14A. The cells range in size from $1 \times 1$ cm to $0.125 \times 0.125$ cm. Four of the smaller cells in a block make up the slit which represents the holes in the thrust barrel. This is discussed in greater detail in simulating the full-scale thrust barrel. The thrust barrel wall is made up of two rows of cells 0.125 cm in thickness which are boundary cells and do not communicate information across the wall. In reviewing the make-up of the grid, it is now apparent that a finer subdivision of cells is needed outside the thrust barrel in the vicinity of the lower curved boundary. The single row of cells here which become filled with liquid did not provide adequate modeling since they were only one row in thickness and were all surface cells with empty cells above. However, when these were subdivided for Case 3, other problems in communication arose which will be discussed in Case 3. The inadequacy of arbitrary boundary modeling with thin films was uncovered in this case and was not solvable here or in Case 3.

Flow progressed down the outer side wall in a satisfactory manner. The use of surface tension/contact angle logic on curved boundaries was demonstrated for the first time in a model simulation. Leading edge velocities were comparable to expected velocities, in a range of 0.8 to 1.0 of free-fall velocity. At 0.40 seconds, the maximum velocity vector was 20 cm/sec. No comparison with test data is available since the resolution of flow in the curved wall drop tower test containers is not of adequate clarity to present here; additionally, flow into the thrust barrel was not adequately defined in drop tower tests for quantitative comparison. After some difficulties were resolved with velocities on open cell faces near the curved boundary and the thrust barrel, flow did cover the lower hole and started to fill the thrust barrel. Flow moved up the side of the thrust barrel at a velocity of about 15 cm/sec and passed above the thrust barrel at 0.72 sec. The thrust barrel commenced filling at 0.60 sec and continued to fill until the end of simulation at 0.77 sec. Velocities through the slit were relatively constant during this period, ranging from 12 to 16 cm/sec. At this rate of filling, the thrust barrel would be half full in 0.5 seconds from start of filling. This compares to a full-scale fill-time for half full of

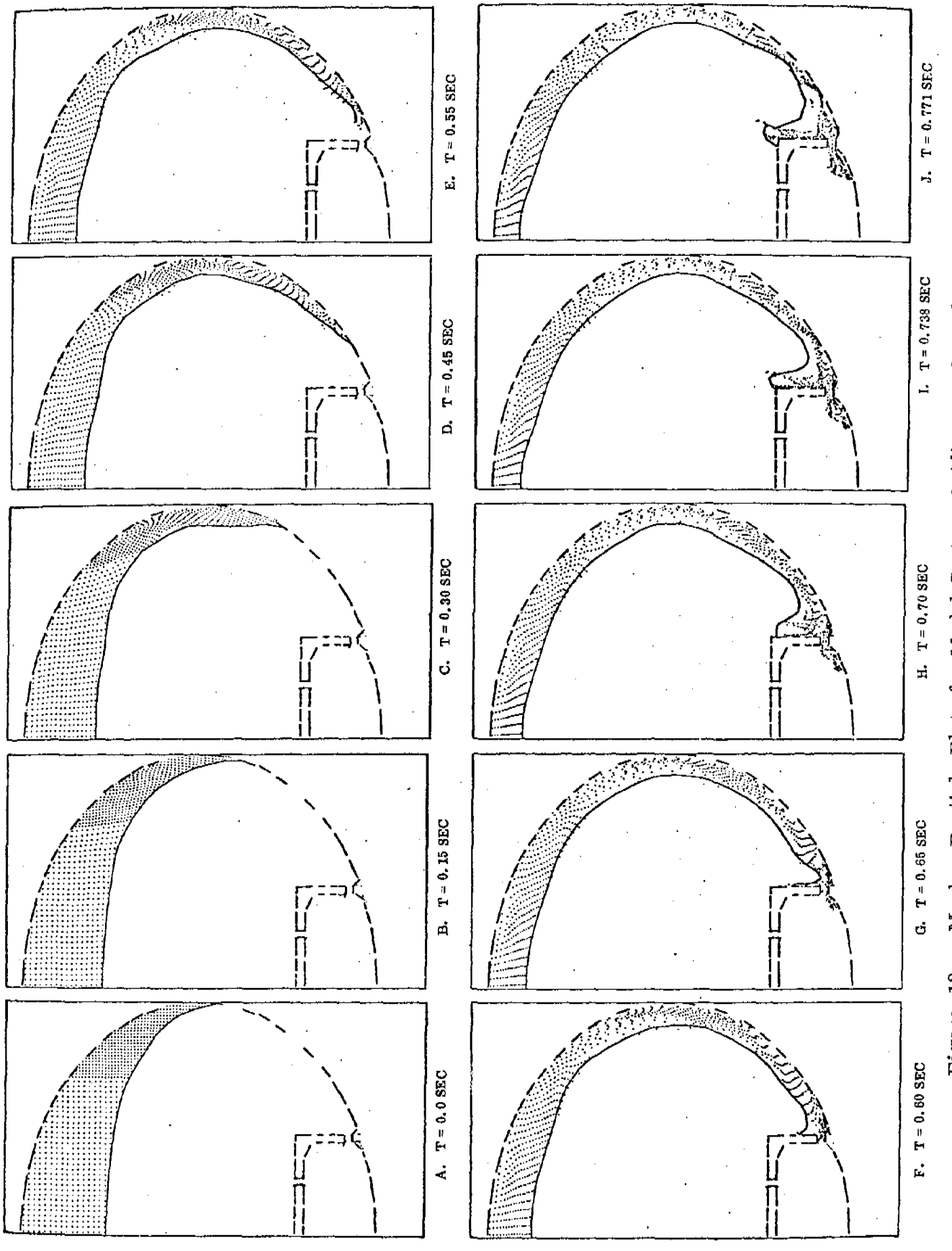


Figure 13. Marker Particle Plots for Model Centaur Oxidizer Tank Settling, Case 2



REPRODUCIBILITY OF THE
ORIGINAL PAGE IS POOR

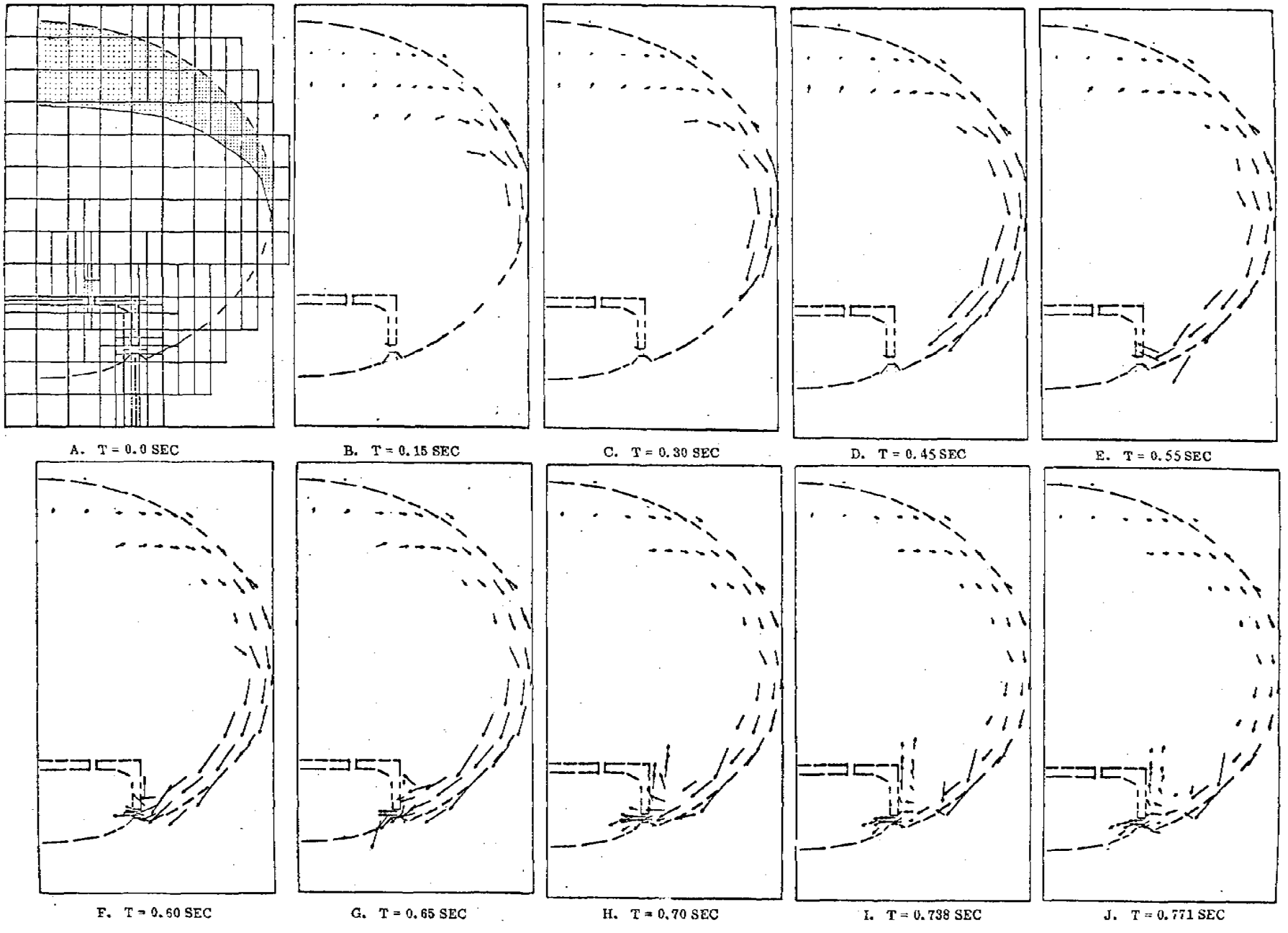


Figure 14. Velocity Vector Plots for Model Centaur Oxidizer Tank Settling, Case 2

approximately 25 seconds. The results of this simulation indicated the potential for Centaur oxidizer tank modeling, and simulation activities proceeded to Case 3, the full-scale tank.

## 3.3 CENTAUR $LO_2$ TANK SETTLING FULL-SCALE - CASE 3

A new grid structure was developed to model the full-scale Centaur oxidizer tank. Foremost, improved modeling of the flow along the lower bulkhead was required. Resolution cell-size was inadequate in Case 2. It was apparent that more cells had to be full, i.e., the film had to occupy more than one layer. It was also desirable to modify the location of the thrust barrel side-hole in relation to the wall such that flow would not occur directly into the hole. It was correctly anticipated that the film along the wall in Case 3 would be thinner due to lower initial liquid residual and that it would turn the corner on reaching the thrust barrel. It was also desirable to improve the modeling of the thrust barrel in line with moving the hole up the side. The dimensions of the thrust barrel are shown in Figure 12B. Three slits (annuli) were used to simulate the hole areas. By moving them radially, the correct area could be achieved for top holes. The marker particle plots for this simulation are presented in Figure 15 and the velocity vectors in Figure 16. The full-scale grid configuration is shown in Figure 16A. The full-scale tank was shown earlier in Figure 11.

The full-scale tank was represented with 390 cells and 430 particles. Cells ranged in size from $1 \times 1$ cm to $0.0625 \times 0.0625$ cm, the latter used to represent the thrust barrel holes. A scale factor of 21.7584 was used to scale the problem to full size. Top slits were made up of four small cells (0.125 cm total) whereas the side slit was 0.0625 cm (unscaled) and only a one by two horizontal array. As evidenced in Figure 16A, the grid in the vicinity of the lower bulkhead is essentially rectangular with good resolution of cells.

The interface shape for the 9 percent liquid present with Bo = 15 was obtained from Concus (Ref. 12) by interpolation for shapes between 12 percent liquid and no liquid and between Bond numbers of 10 and 30. The flow was initiated with surface tension logic active and a wall contact angle of 20°, which was measured from a surface marker particle at the center of the nearest boundary cell (Section 2.2.5). The simulation advanced down the sidewall in an uneventful manner. Velocities continued to increase proportional to the settling time. After ten seconds, some anomolies arose with the thin film thickness. Cells one away from the boundary were intermittently voiding and filling as particles moved in and out of them. From this point in time, certain cells had to be continually monitored to maintain them full without neglecting the restriction of maintaining a thin film. This procedure was required along the entire arbitrary boundary to the thrust barrel. Further difficulties developed in the transmission of advance cell velocity and pressure information when the film was only one cell thick in many instances. Extraneous velocities occurred on empty cell faces which were unrealistic and raised doubt in the accuracy of the modeling of thin films such as experienced here. It appeared continuity in flow down the arbitrary boundary could not be obtained, an apparent shortfall in the code. After considerable attempts, solutions were obtained for flow into the corner area formed by the curved bulkhead and the thrust barrel. At 20 seconds, flow reached

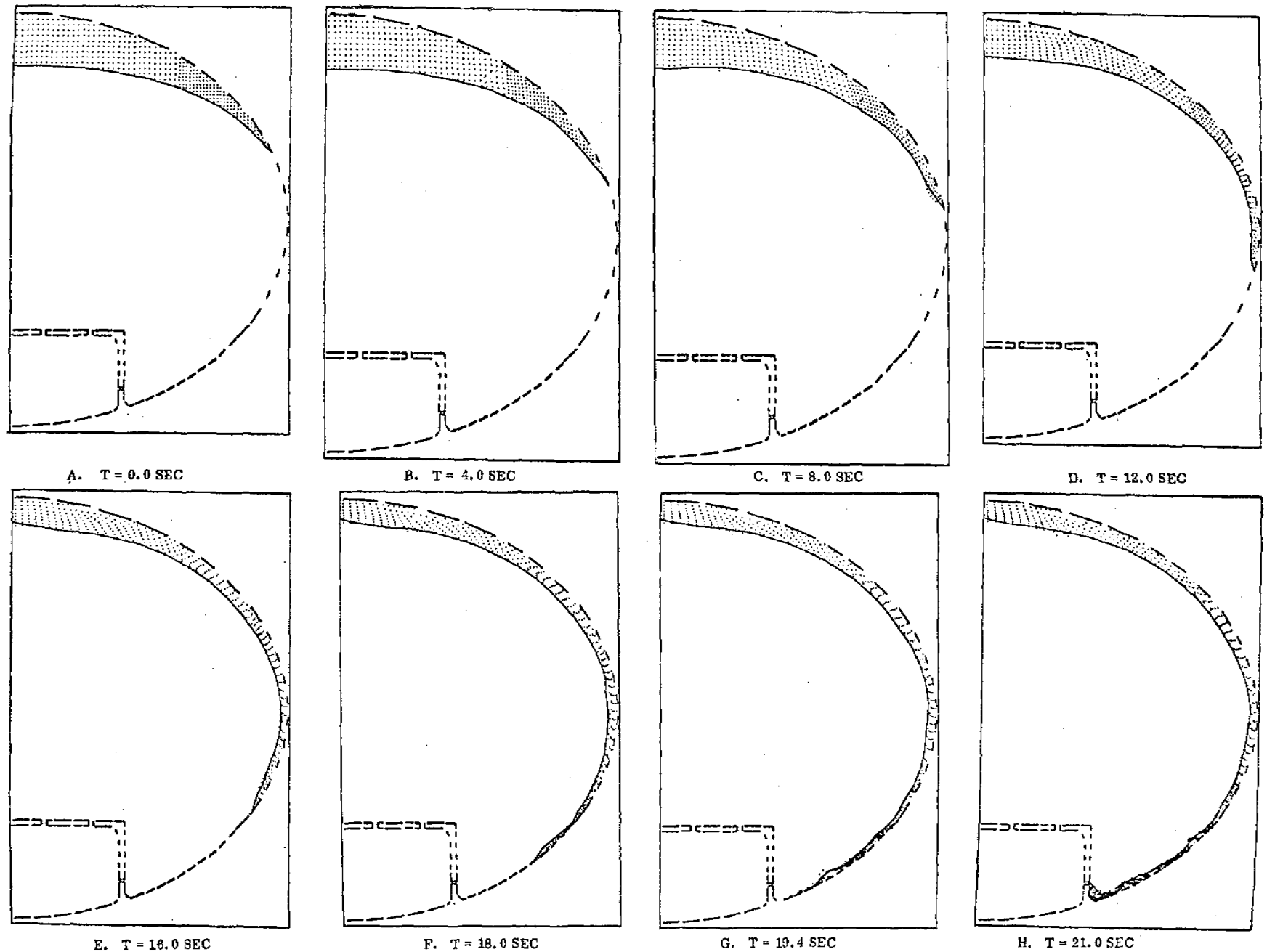


Figure 15. Marker Particle Plots for Full-Scale Centaur Oxidizer Tank Settling, Case 3

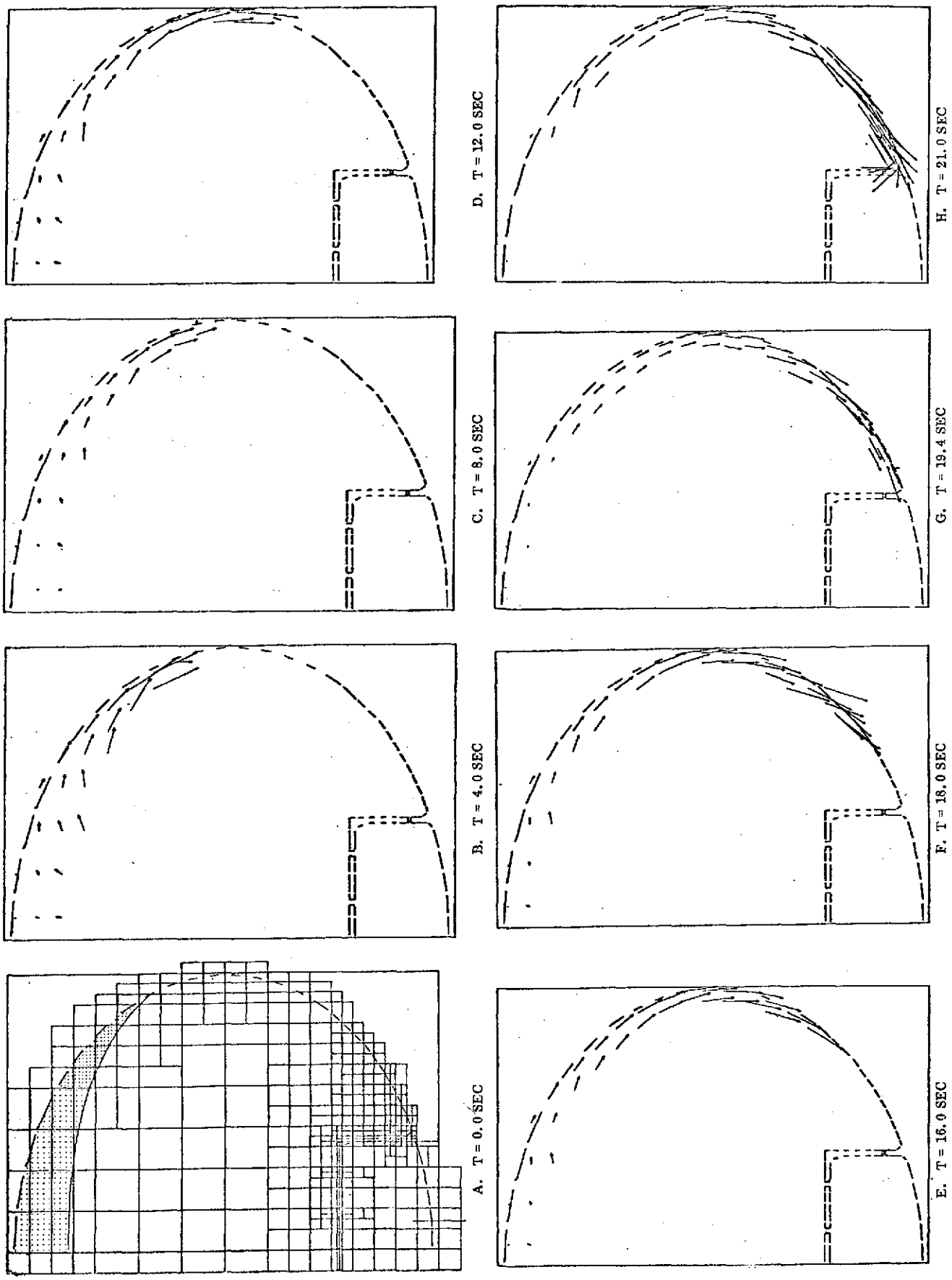


Figure 16. Velocity Vector Plots for Full-Scale Centaur Oxidizer Tank Settling, Case 3

REPRODUCIBILITY OF THE
ORIGINAL PAGE IS POOR

the thrust barrel and turned upward with a full-scale velocity of 20 cm/sec. It is reasonable to assume, from the results of Case 2, that thrust barrel filling would have occurred from this time onward. In light of the discontinuities experienced in the pressure and velocity fields along the boundary, the validity of the results for the pressure field causing flow through the hold are in doubt. The simulation was discontinued since computer runs would only proceed a few steps, less than one-half second, before some velocities along the lower boundary would exceed reasonable values.

It is concluded that without further program modifications, the modeling of flow of extremely thin films of liquids over arbitrary boundaries should not be attempted. Further examination of program logic in these areas with respect to velocity and pressure field propogation is required.

### 3.4 CENTAUR $LH_2$ TANK MIXING - FULL-SCALE - CASE 4

A requirement exists during extended space missions to control cryogenic tankage pressure rise rates caused by fluid stratification. Most concepts currently under consideration utilize a mixer which consists of a jet pump to ensure the fluid in the tank is well-mixed. In reduced-gravity the mixer power requirement to pump liquid from one end of the tank to the interface is much smaller than in one-g. The strength of the jet does not have to overcome the pressure drop resulting from a gravity-produced liquid head. Mixing is also influenced in one-g by density differences, whereas in reduced-gravity these effects are minimized or absent. It is difficult, if not impossible, to maintain a similitude of the appropriate force and flow field variables for the two cases. Hence, one-g simulation of low-power mixing is not necessarily reliable.

Only recently, with drop tower work at the NASA/Lewis Research Center, has low-g fluid jet mixing been investigated experimentally. The marker-and-cell code provides a simulation tool to examine the full-scale mixing problem in reduced gravity fields. This simulation, Case 4, is representative of the potential for acquiring flow field data from such a simulation. The flow field is an adequate indicator of destratification.

3.4.1 SYSTEM SIZING - Previous test results in one-g with cryogenics and water to investigate destratification for space missions afford one source of data for sizing the jet flow. The correlations for mixing from the chemical industry afford a second source of data. In a recent Convair effort (Ref. 13) the above sources were compared and the correlation which best represented available data was selected. To examine the variables and to show the basis of a design criteria, the work of these investigators will be briefly reviewed in chronological order.

Fossett and Prosser (Ref. 14) studied the mixing of a $Na_2CO_2$ solution in a tank with a jet mixer. The emf response of a pair of electrodes in the fluid to be mixed relative to a second pair in a homogeneous fluid were the measure of mixing. In their data analysis, they determined a mixing factor which was independent of the jet Reynolds number. Their correlation for the mixing factor is a constant of 9 resulting in

$$\theta_m V_j D_j / D_t^2 = 9 \qquad (32)$$

where

$\theta_m$ = mixing time in sec

$V_j$ = exit jet velocity, ft/sec

$D_j$ = jet exit diameter, ft

$D_t$ = tank diameter, ft

The data from tests performed with four different configurations and fluids to analyze fluid mixing in aerospace applications is plotted in Figure 17 along with the above correlation. The correlation is adequate in view of data scatter but points up a potential inadequacy of their defined mixing factor.

Recognizing this deficiency in the above correlation factor, Fox and Gex (Ref. 15) proposed a more complex factor to correlate their test results. Their experimental

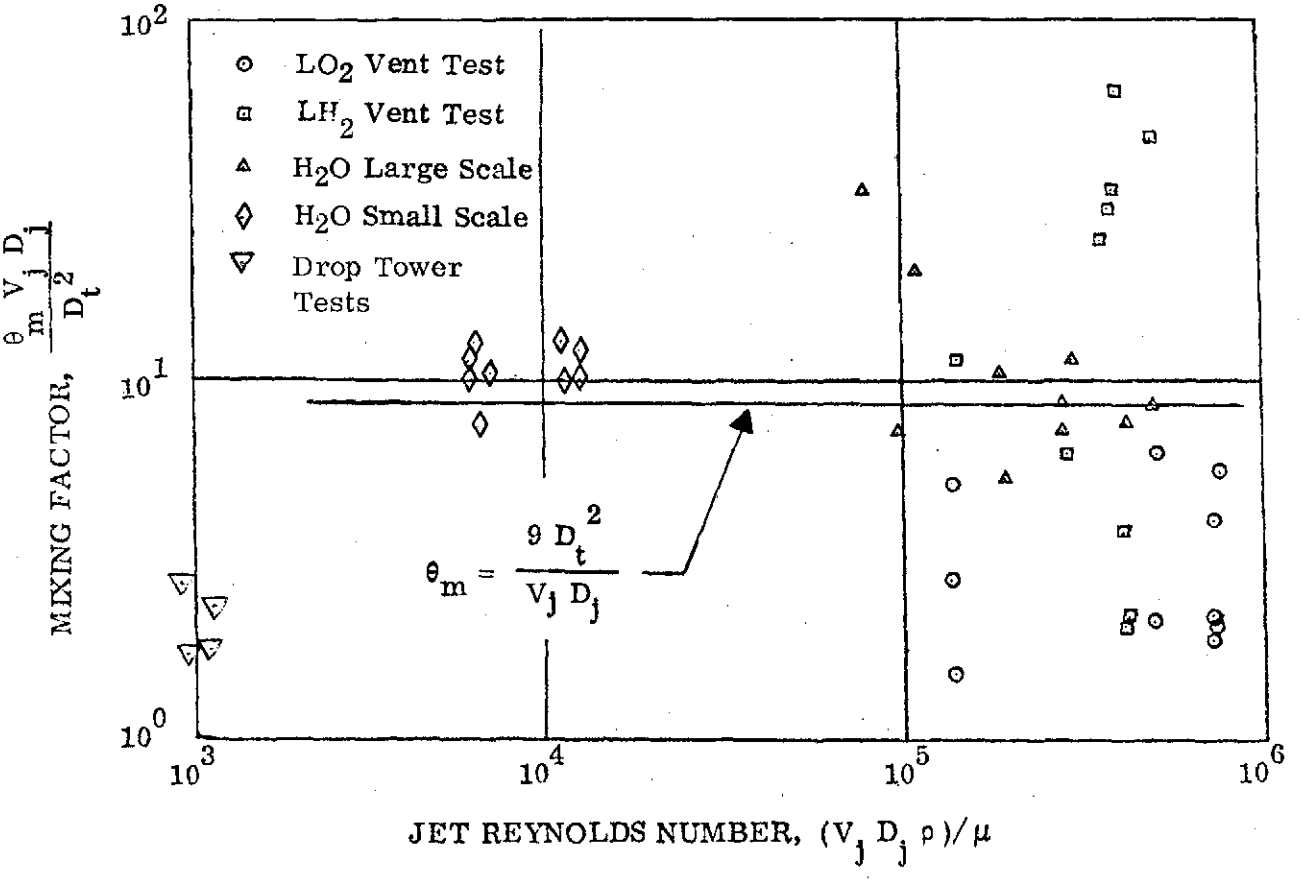


Figure 17. Data Correlation for Selection of Mixing Factor, Equation by Fossett and Prosser

data was obtained from jet mixing of a known acidic solution into a tank of basic solution containing an acid-base indicator. Their correlation is presented in Figure 18 where it is noted the laminar jet regime ends at $Re_j = 2000$ and the turbulent region employs a different correlation. Only the turbulent regime is of interest here. Their work, in agreement with the above, suggests the parameter $V_j D_j$ to be the key variable. For the turbulent regime, they also include the liquid height and jet Reynolds number

$$\frac{\theta_m (V_j D_j)^{4/6} g^{1/6}}{Y^{1/2} D_t} = 118 \, Re_j^{-1/6} \tag{33}$$

where

g = the gravitational acceleration, $ft/sec^2$

Y = liquid depth, ft

The use of g as a low-g variable acceleration field rather than a conversion constant is questionable. Results in Figure 18 indicate a higher constant than 118 is required to fit the data, i.e., mixing times are two-to-four-fold that predicted with this correlation.

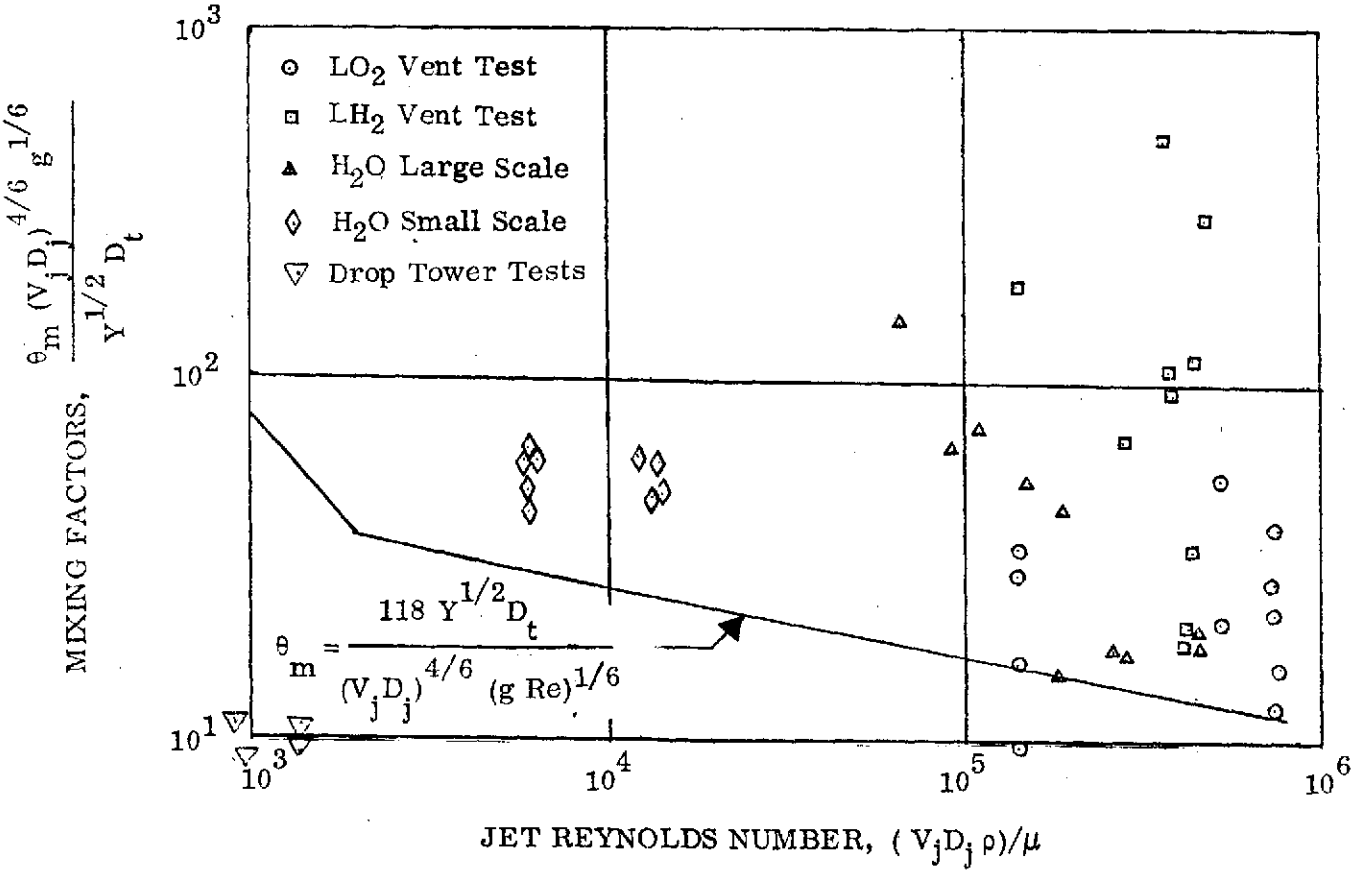


Figure 18. Data Correlation for Selection of Mixing Factor, Equation by Fox and Gex

The preferred correlation for mixing time is that presented by Okita and Oyama (Ref. 16). Their mixing tests were also of a chemical nature and required establishing equal potential readings in NaCl solutions. In correlating results they defined a mixing factor which was independent of jet Reynolds number for $Re > 5 \times 10^{-3}$ of the form

$$\frac{\theta_m Q Y^{1/2} D_t^{1/2}}{V_L D_j} = 5.2 \tag{34}$$

where

$Q$ = volumetric flowrate, $V_j \pi D_j^2 / 4$

$V_L$ = liquid volume ~ $Y \pi D_t^2 / 4$

Formulated in a manner similar to the above investigators

$$\frac{\theta_m (D_j V_j)}{Y^{1/2} D_t^{3/2}} = 5.2 \tag{35}$$

The data correlation is presented in Figure 19. Since it significantly reduces scatter and is the most conservative of the three correlations at high jet Reynolds numbers, it was used for defining mixer variables in the marker-and-cell Case 4 simulation.

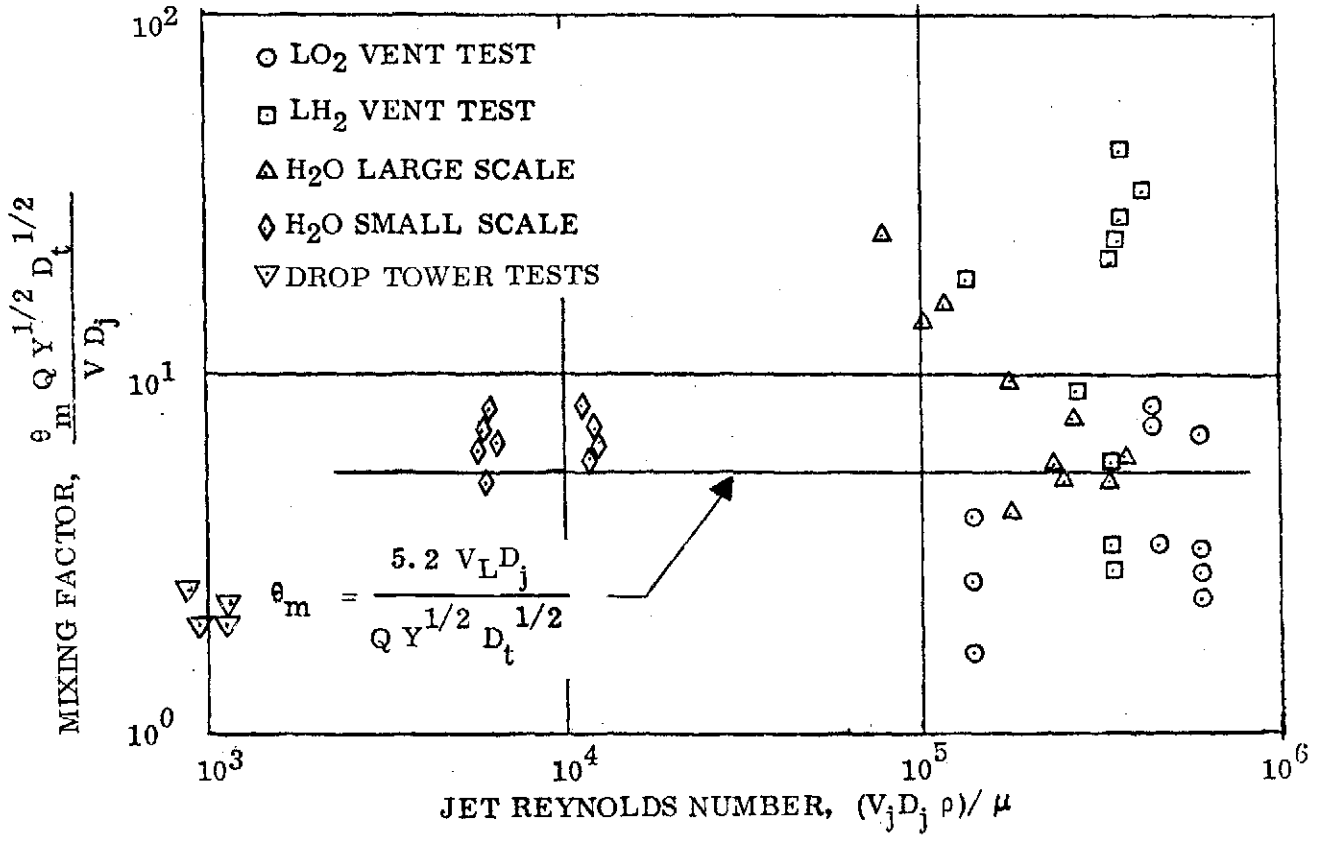


Figure 19. Data Correlation for Selection of Mixing Factor, Equation by Okita and Oyama



REPRODUCIBILITY OF THE

Another investigator evaluated the effect of the jet on the interface as it affects interfacial mixing. Jet mixing was evaluated by Poth (Ref. 17) with water heated by wall heaters to develop a stratified layer which could be broken-up with a given strength jet. A criterion was theoretically established defining a critical Weber number such that mixer exit velocities in excess of this value would result in interface break-up. The correlation which was theoretically arrived at is

$$We_{crit} = V_j^2 D_j / \beta = 1.055\ Y / D_j \qquad (36)$$

for Bond numbers in the range $-10 < Bo_{d,t} < 10$. For a liquid height Y of 300 cm and $D_j = 12$ cm in the current study, the value for $We_{crit} = 26$ is independent of Bond number.

There are, however, further considerations on the acceleration environment in the determination of ullage break-up from a submerged liquid jet. Poth comments that above a Bond number of 10, a Froude number criteria must also be considered (Ref. 17). This Froude number criteria was derived for a tank with $L/D_t$ of 2 for conditions for a submerged jet to reach the upper bulkhead. The criteria is presented (Ref. 17) in terms of Froude number

$$Fr_{crit} = V_j^2 / g D_t = 0.422 (D_t/D_j)^2 \qquad (37)$$

Considering the dimensions of the Centaur tank and the 12 cm jet outlet proposed above, the critical Froude number is 272.

The critical Froude number criteria can also be expressed in terms of the jet critical Weber number as a function of the Bond number. With appropriate substitution and a change from tank diameter to tank radius for the Bond number ($g r_t^2/\beta$)

$$We_{crit} = 1.688 (D_t/D_j) Bo_{r,t} \qquad (38)$$

The change in limits for the two correlations is $Bo_{r,t} = 2.5$ rather than Bo = 10 above based on tank diameter. To consider this transition between the two correlations, they are plotted in Figure 20. It is apparent that a transition zone is required between the two correlations; however, the influence of the acceleration field is significant to a Bond number below 1.

Some preliminary results from recent drop tower tests at NASA Lewis Research Center (Ref. 18) represent the only available low-g mixer data. Their work was performed in a 10 cm diameter cylinder with flow into the cylinder through an 0.4 cm diameter jet colored by dye. Their results in very low-g verified the Weber number correlation for interface break-up. In tests where jet velocities did not exceed the critical Weber number, the flow patterns reached the interface and flowed laterally to the side wall and did not break the interface. The length of the drop did not provide adequate viewing

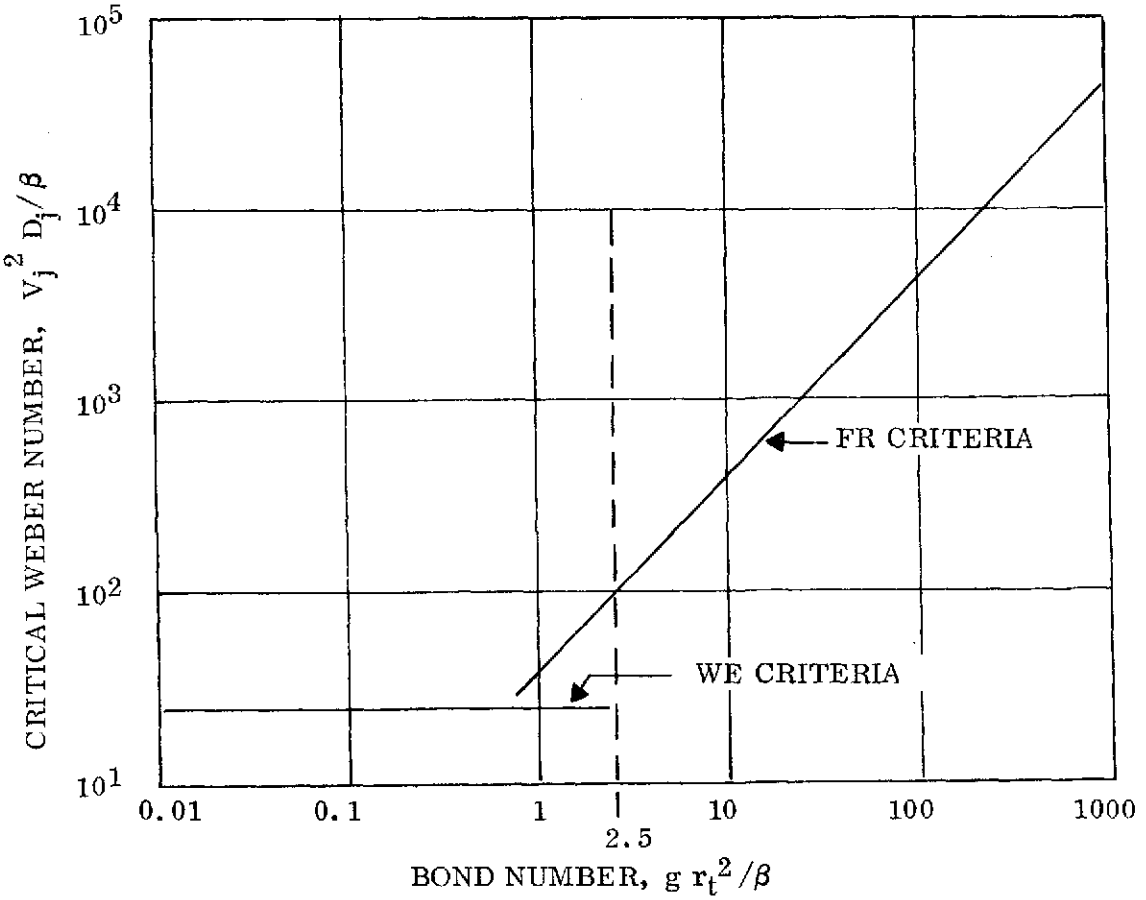


Figure 20. Weber and Froude Number Criteria for Interface Breakup

time for dye trace evaluation of vortices or flow contact with the wall. Future tests at low thrust (finite drag Bond numbers) would provide the much needed verification of the critical Froude number criteria.

In sizing the mixer for this full-scale Centaur fuel tank simulation, the criteria of Okita for mixing time and of Poth for a critical Weber number defining interface break-up were considered. The design procedure that follows is for a Bond number less than one using Equation 36 since the authors were unaware of the more restrictive criteria imposed at higher Bond numbers by the Froude number criteria. Since liquid depth above the mixer was specified as 300 cm with a tank diameter of 304.8 cm, the two equations can be solved simultaneously if a factor $\alpha$ is introduced for the number of times above $We_{crit}$ that is selected for operation. In this series of trial and error calculations on two equations, the following variables are optimized: maximize turnover, minimize mixing time, maximize $\alpha$ to assure interface break-up within the constraints of a low velocity jet with a reasonable diameter, say 12 cm. It was preferred to simulate low velocity jets since high velocities reduce time-steps in the marker-and-cell technique. The chosen operational variables are summarized in Table II.



REPRODUCIBILITY OF THE
ORIGINAL PAGE IS POOR

TABLE II. DESIGN VARIABLES FOR CENTAUR FUEL TANK MIXER - CASE 4

| | | | |
|---|---|---|---|
| $V_L$ | = $21.6 \times 10^6$ cm$^3$ (60% liq.) | $Re_j$ | = $1.06 \times 10^5$ |
| $D_t$ | = 304.8 cm | $We_{crit}$ | = 26.4 |
| Y | = 300 cm | $We_{act}$ | = 132.7* |
| $\beta$ | = 27.07 cm$^3$/sec$^2$ | $Fr_{crit}$ | = 272 |
| $D_j$ | = 12 cm | $Fr_{act}$ | = 56* |
| $V_j$ | = 17.3 cm/sec | Q | = 1956.6 cm$^3$/sec |
| g | = + 0.0174* cm/sec$^2$ | $\theta_m$ | = 2281 sec |
| Bo | = 15* | $\theta_t$ | = 11040 sec per volumetric turnover |

* It will be pointed out later that an acceleration field of 0.116 with Bo of 100 was finally used.

The data on volume turnovers is presented since this is a correlation variable for some authors. For a given diameter jet the mixing times of the first three authors above reduce to fractional volume turnover equivalents of 0.358, 0.073, and 0.207, respectively; i.e. this volume turnover has occurred in the predicted time for mixing, $\theta_m$. The considerable extent of disagreement between workers is obvious. In Reference 13, Convair experienced tank homogeniety with $LO_2$ in a range from 0.024 to 0.26 turnovers suggesting the non-reliability of this statistic. For the Case 4 simulation this would suggest mixing times of 265 to 2870 sec.

Once the mixer variables were determined, the details of establishing the grid for the problem were defined next. As indicated earlier, high velocities in a cell result in small time-steps because of time-step criteria in the computer code which limit particle travel to one-half a cell dimension. If the exit of the mixer, 6 cm radius, were used as a cell dimension with, for example, a 12 cm height, the time step would still be limited to 12 cm/(2 · 17.3 cm/sec) or 0.347 seconds. A solution to this was to use a large cell dimension for the mixer and, using the continuity equation and existing data on jet spread angle and entrainment, to determine the equivalent cell inlet and outlet velocities. From previous experience with the Centaur hydrogen tank, a cell-size of 152.4/24 cm in width (10.886 cm) by 152.4/7 cm in height (21.772 cm) was selected.

The literature on axisymmetric submerged jets in an incompressible fluid provided data on the spread of the jet and the entrained fluid (Ref. 19). The jet spread angle is 15°. Thus within one cell length the 6 cm outlet radii can be represented by flow out a cell width. The fluid entrained by the jet is a function of the distance from the exit. These regions are defined as initial, which exists for 9 jet radii, a transition region, and a main region which starts at about 20 jet radii. In the initial region, the entrainment is determined from

$$Q' = Q_o\,(1 + 0.073\,\bar{x} + 0.002\,\bar{x}^2 = .0001\,\bar{x}^3 + .000002\,\bar{x}^4) \qquad (39)$$

where

$Q'$ = volumetric flowrate at a distance $\bar{x}$

$Q_o$ = exit volumetric flowrate

$\bar{x}$ = $x/r_o$ with $r_o$ nozzle radius

$x$ = centerline distance from the nozzle exit

In the main region, the expression is simply

$$Q = Q_o\,(0.155\,\bar{x}) \qquad (40)$$

The first equation was used to determine entrainment within the mixer cell with $Q'/Q_o$ = 1.28. The equivalent inlet velocity at the top of the cell (Figure 21) is -5.256 cm/sec, the cell side velocity for the cylindrical sidewall surface is -0.377 cm/sec representing entrainment producing an outlet flow of -6.763 cm/sec. This latter value permitted a time step of 21.77 cm/(2 · 6.763 cm/sec) or 1.61 sec. This was extended to 2 second steps since the flow in this region was predictable and cell voiding below the mixer was not a problem.

3.4.2 MIXING SIMULATION - The physical characteristics of this full-scale $LH_2$ tank simulation were a 60% liquid-fill case represented by the grid configuration shown in Figure 23A and made up of 360 cells with initially 2407 particles. The basic grid dimension was 1 cm × 1 cm with a scale factor of 21.7714, with sub-divisions of this basic grid. The gravity level was initially -0.0174 cm/sec$^2$ representing a Bond number due to drag of 15; however, this proved unsatisfactory and an acceleration of 0.116 cm/sec ($1.2 \times 10^{-4}$ g's) was selected (Bo = 100). The problem of non-convergence arose at the low Bond number and it was decided that the demonstration of mixing flow fields would also be of interest at a higher Bond number. This non-convergence problem exists due to the lack of well-defined pressure field; comments on Case 1 apply here also.

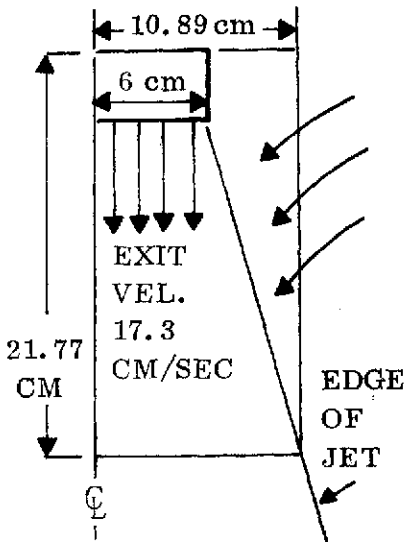


Figure 21. Simulated Mixer Cell

For the initial selected Bond number of 15, the critical Weber number is 640, and for the Bond number of 100 which was used, $We_{j,crit}$ = 4300. Since the Froude number is a significant factor in the ullage break-up, the jet momentum was insufficient to break the interface. Nonetheless, mixing in low earth orbit remains to be of considerable interest where drag Bond numbers in the

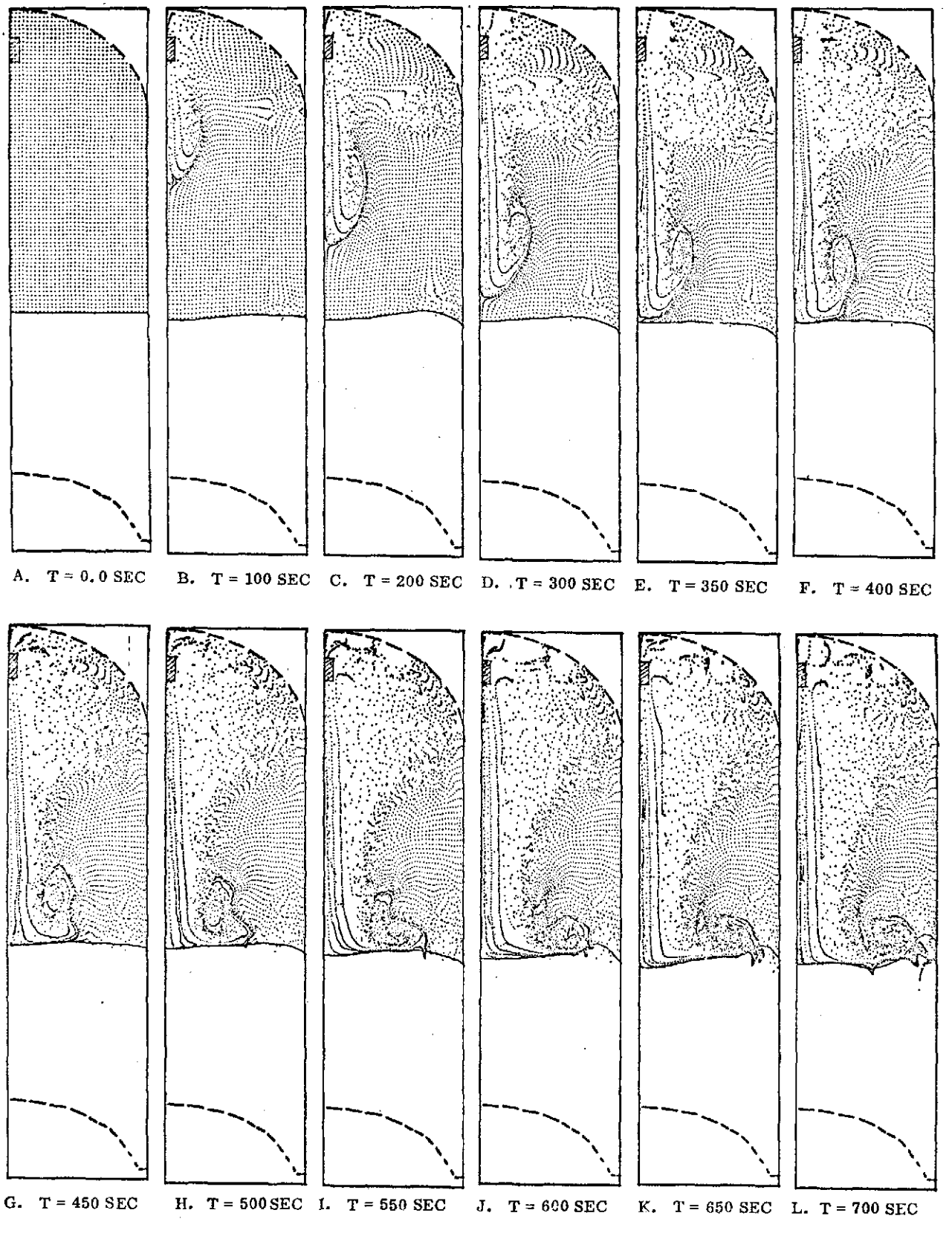


Figure 22. Marker Particle Plots for Full-Scale Centaur Fuel Tank Mixing Simulation in Low-g, Case 4



REPRODUCIBILITY OF THE
ORIGINAL PAGE IS POOR

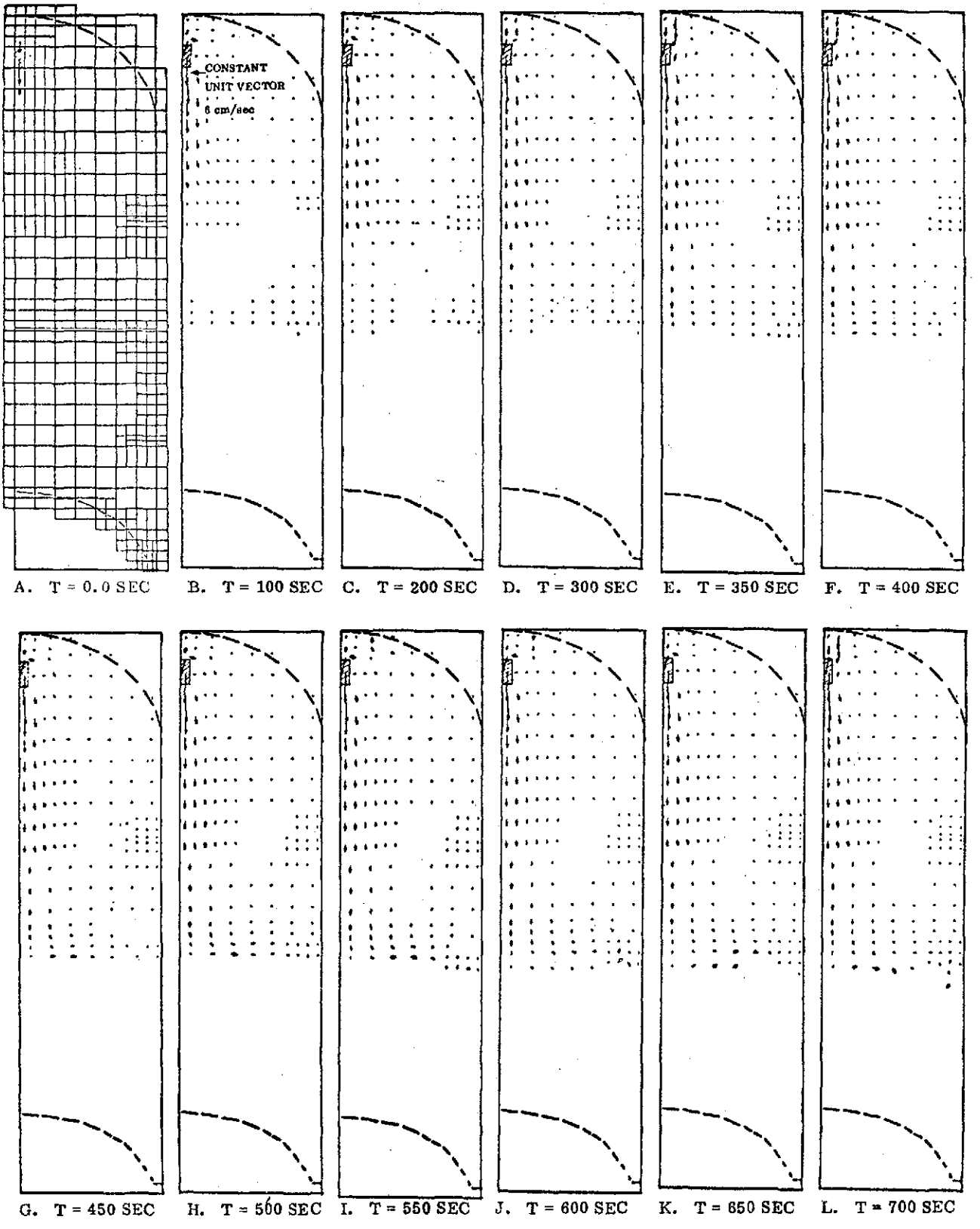


Figure 23. Velocity Vector Plots for Full-Scale Centaur Fuel Tank Mixing Simulation in Low-g, Case 4

range 5 to 100 are applicable. With the low mixer exit velocities selected here based on the Weber number criteria at low Bond number, interface breakup could not be verified because the Froude number criterion was unsatisfied. The flow conditions modeled can still indicate the potential for effective destruction of stratification at the interface due to the interface velocities.

A second problem in the initial set-up was the interface for a Bond number of 100. This interface appeared to be unstable, even with surface tension logic in use. Initial surface velocities (instabilities) developed near the wall independent of mixer flow which would have masked later mixer flow at the interface. It is assumed a balance of forces did not exist. This was resolved with the adoption of a flat interface as illustrated in Figure 22A.

The simulation proceeded smoothly with cells acquiring velocities as the mixing front moved forward. The Marker particle plots are shown in Figure 22 for representative times from 0 to 700 seconds mixing time. Initially, particles were added each step to three locations near the mixer to preclude cell voiding. It became apparent that other locations later in the problem also had to have particle addition to avoid empty cells which were really full. The initial addition provides a useful pattern similar to dye or smoke to follow the leading velocity front. This figure shows an interface instability which developed late in the problem and resembled a surface wave. The interface velocities by 700 seconds are sufficiently strong to ensure interface mixing.

The velocity vectors for the same time period are presented in Figure 23. This group of plots are unique in that velocities are comparable since the maximum velocity on all of the plots (6.0 cm/sec at the center of the mixer cell) was held constant. The velocities throughout the tank increase with time and approach a steady-state condition. The velocity vectors indicate the vortices formed in the tank. A well-defined path down the centerline and across the interface, as well as the expansion of the jet, is indicated. The nearly horizontal flow below the mixer raises an area of interest. Since the velocities in most of the tank are small relative to the mixer inlet velocity, a change in scale was introduced for duplicate plots after 300 seconds. This magnifies all vectors by 15 and provides improved resolution for examination of interface velocities. These vector plots are shown in Figure 24.

The magnitude of velocity vectors are plotted at specific tank locations as presented in Figures 25 and 26. These locations are considered to evaluate the approach to steady-state mixing flow conditions in the tank. The velocities along the centerline described in Figure 25 are well-behaved and remain relatively constant once flow is established at that location. The diminishing strength of the jet with distance from the nozzle is easily detected. In Figure 26, the velocities show larger perturbations due to interface instabilities, however a definite trend toward steady-state is observed. The absolute value of these vectors is not so important as the trend they present for the mixing capability of this type of flow. An approximation of less than 450 seconds for the mixer flow to progress down the centerline and to the tank wall is a logical conclusion. A further conclusion is the adequacy of this flow to reduce stratification in a period less than predicted by the correlations of Okita.

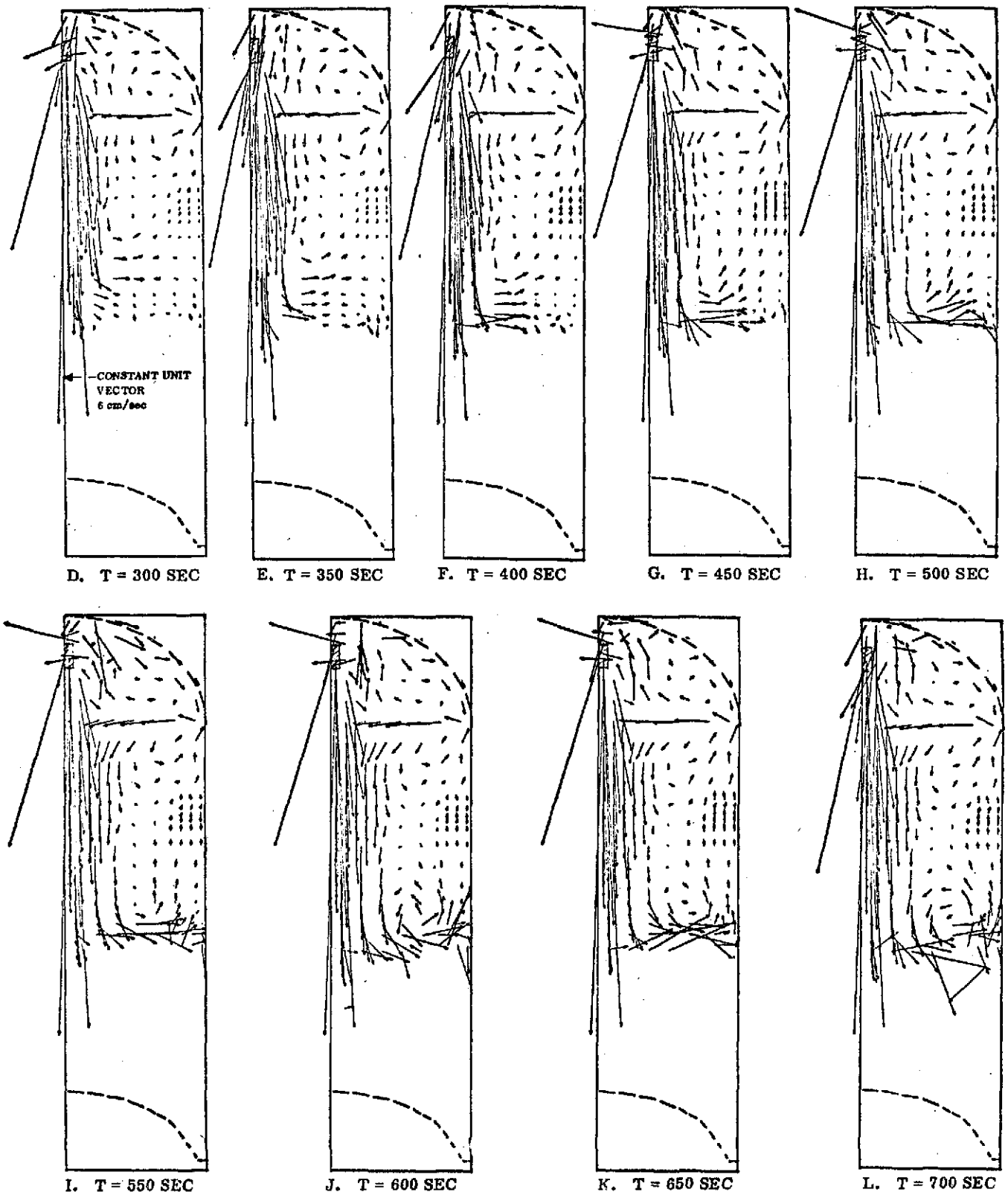


Figure 24. Magnified Velocity Vector Plots for Full-Scale Fuel Tank Mixing Simulation in Low-g, Case 4



REPRODUCIBILITY OF THE ORIGINAL PAGE IS POOR

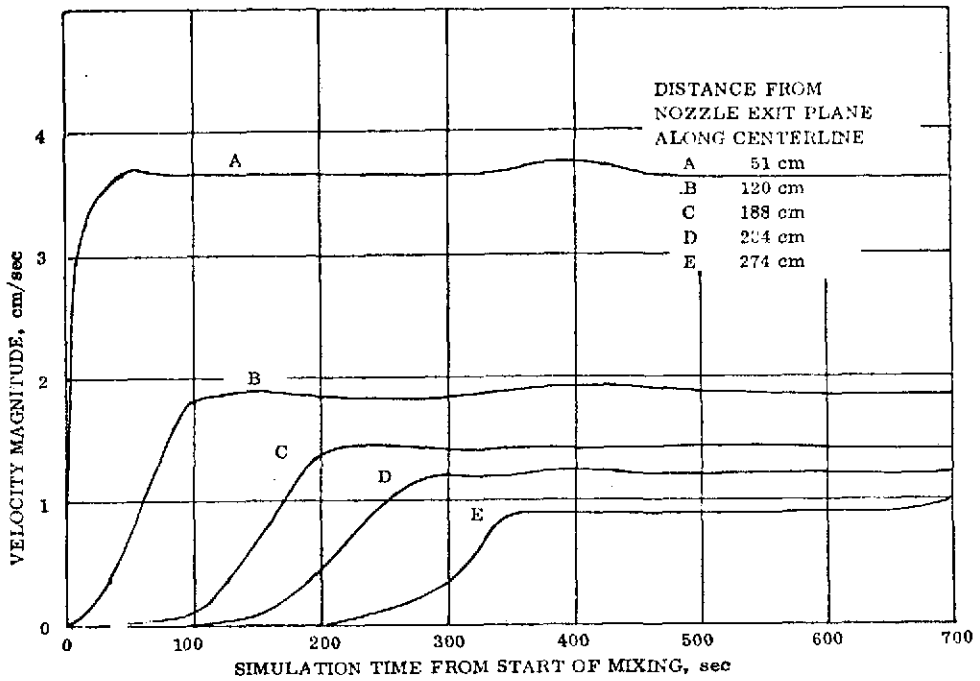


Figure 25. Magnitude of Velocity at Several Distances From Nozzle Exit Plane

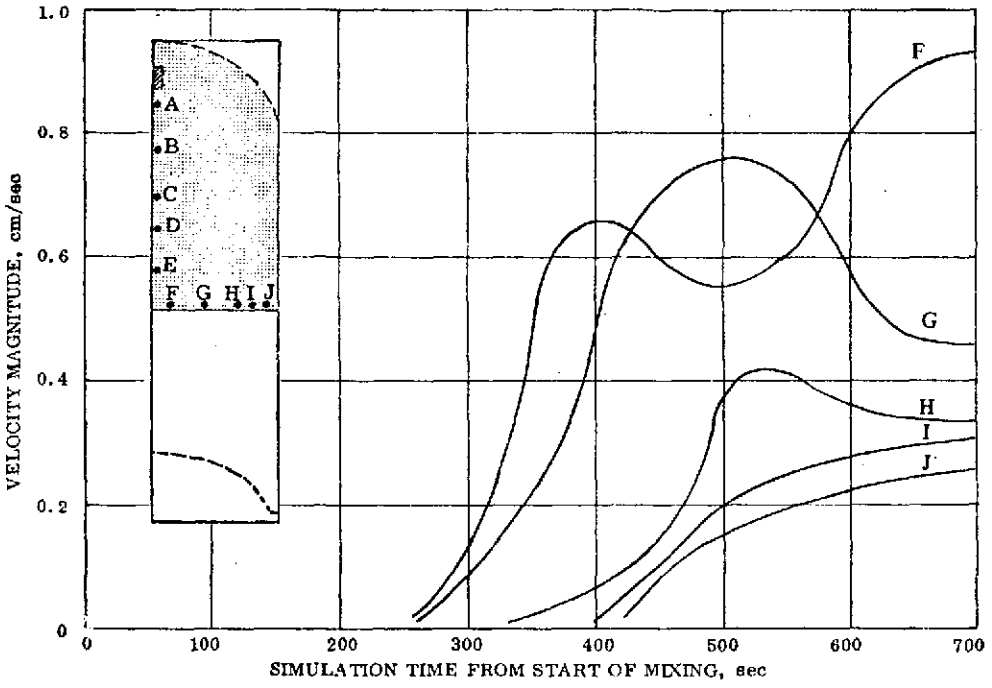


Figure 26. Magnitude of Surface Velocities at Radial Locations

The marker-and-cell code was shown to be a useful design tool for the analysis of mixer location and mixer flow patterns. This simulation method affords an economical approach to the analysis of full-scale mixing flows.

# 4

## CONCLUSIONS AND RECOMMENDATIONS

Extensive logic to consider surface tension forces which used a spline fit to a monotonic series of surface points was successfully added to the marker-and-cell code ERIE. This logic further includes end conditions which permit the simulation of contact angles on straight walls, as well as both concave and convex walls. The accuracy of this logic was verified for specific liquid interfaces, for test cases and in four simulation cases covering a range of gravity levels. These four cases were the primary emphasis for this study. Case 1 involved the simulation of impulsive settling for a Centaur model $LH_2$ tank; Cases 2 and 3 respectively considered model and full-scale Centaur $LO_2$ tank continuous settling; finally Case 4 simulated mixing in a full-scale Centaur $LH_2$ tank.

A detailed examination of convergence procedures in code ERIE was required to alleviate the extensive iterations which occur when the simulation does not contain a significant acceleration field and the pressure gradient in the tank is small. Two new convergence methods were concluded to be less effective than the existing method. Therefore, the current method was improved with the addition of an extrapolation technique for the pressure field. This was based on the magnitude of the change in three successive iterates every 40 steps in the iteration. This procedure worked effectively in all cases at both high and low gravity levels although further improvements are still needed. Convergence at reduced gravity levels remains a major area for improvement in this code. It must be concluded that the solution to improved convergence which permitted the modeling of impulsive-g was not of universal application to cover acceleration environments required for mixing simulations.

The impulsive settling Case 1 was a partial success in that simulation continued for 1.88 seconds through more than half of the settling flow. An unexpected stall of the flow along the lower bulkhead for one-half second could not be explained. This delay and convergence difficulties prevented computation of this case to the desired 3 seconds. At that time, flow had stagnated and surface tension forces were dominant in returning the fluid to an equilibrium configuration. Our results did indicate an expected decay of velocity after the decrease in the acceleration field. The marker-and-cell code is ideally suited for this analysis in that the acceleration field can be easily changed. The new version of the code models the significant force of surface tension, and the flow simulation is not only graphically given, but the magnitude of local velocities may be assessed.

The simulation of the Centaur $LO_2$ tank indicated the code ERIE could be used for detailed simulation. The flow into the thrust barrel through ports represented a new dimension in modeling. The case made extensive use of the variable grid capability with a wide range of cell sizes, this case also made extensive use of arbitrary

boundaries. In Case 2 Centaur $LO_2$ tank drop tower model simulation was achieved through 0.77 seconds which was adequate to demonstrate settling flow down the aft bulkhead and up the side of the thrust barrel. Flow into the thrust barrel through side ports was adequately simulated and an estimate of fill rates and times was determined. Flow difficulties along the aft curved boundary precluded the investigation of flow on top of the thrust barrel.

In Case 3, the full-scale Centaur $LO_2$ tank simulation, flow down the aft bulkhead was achieved for a simulation of 9 percent liquid present for 21 sec when flow reached the thrust barrel. Flow simulation only reached the bottom holes of the thrust barrel. The thin film occurring with the little liquid present resulted in more complex simulation problems than with Case 2 for 30 percent liquid. Unrealistically high velocities were being defined on the aft bulkhead due to the thin film and continuation of the case was impractical. It was concluded that the logic in the program depends upon a communication of pressure and velocity through full cells which cannot be satisfied by a single row of cells containing fluid along an arbitrary boundary. Modeling was not improved with the use of finer cell divisions after Case 2. It is concluded that code modifications will be required before satisfactory modeling of thin films on arbitrary curved boundaries can be achieved.

The results of Case 4 confirmed mixing expectations. The case demonstrated the capability of the marker-and-cell code ERIE to simulate reduced-gravity mixing. The simulation was stopped at 700 seconds when steady-state conditions were realized. The flow patterns developed in a logical manner and reached steady-state in a time less than was predicted from available correlations for total mixing. The velocity vectors along the interface were strong and indicated the mixer flow had reached the wall prior to 700 seconds. This flow from the mixer to the interface would result in destratification. Theoretical predictions for interface break-up indicated jet momentum would be insufficient to break-up the interface and this was proven to be true. Some minor wave motion and instabilities approaching the wall were characteristics of the final interface behavior. The inability to gain convergence on mixing at low Bond numbers is not understood with respect to the results of Case 1. The mixing correlations appear to be conservative if the criterion is pressure decay caused by cold fluid from the mixer replacing the interface fluid. Earlier investigations were concerned with total tank homogenity. Case 4 did demonstrate the capability of this code to model mixing at a low cost.

It is recommended that additional work be done to improve the convergence of this code for low-g simulation where the pressure gradient is small. This would be productive in examination of mixing at lower Bond numbers and with stronger jets; i.e., higher jet exit velocities. The final Case 4 would not converge at low gravity levels. Therefore, a higher gravity level was attempted for Case 4 than in the impulsive-g Case 1. The temporary solution was to increase the gravity level from Bo = 15 to 100, however, this would not be satisfactory for cases which should be modeled at Bond numbers 0.1 to 10. The results of impulsive-g settling indicate the promise of the efficiency

of such a settling approach. This code can examine sequencing and optimum thrust application for full-scale simulations. The new capability of the code with surface tension forces opens several areas of low-g fluid motion for examination: impulsive settling, fluid mixing during coast and surface tension driven flows.

## APPENDIX A

## NOMENCLATURE

| | |
|---|---|
| Bo | Bond number, $g_z\, r_t^2 / \beta$ |
| c | wave speed |
| D | velocity divergence = $(1/r^{\alpha})\ (\partial\, r^{\alpha} u/\partial r) + (\partial v/\partial z)$, distance |
| D | diameter |
| EPS | convergence criteria |
| G | cell flag |
| $g_r$ | radial acceleration |
| $g_z$ | axial acceleration |
| h | height of liquid |
| $\hat{n}$ | unit normal defining a boundary segment |
| P | pressure, $L^2\, T^{-2}$ |
| Q | jet volumetric flow rate |
| r | radial coordinate |
| R | radial distance to center or side of cell determined by subscript |
| $R_1$, $R_2$ | radius of curvature |
| $Re_j$ | jet Reynolds number |
| t | time |
| u | radial component of velocity |
| $\tilde{u}$ | radial storage variable, radial component of the tilde velocity |
| v | axial component of velocity |
| $\tilde{v}$ | axial storage variable, axial component of the tilde velocity |
| $\vec{V}_M$ | liquid velocity at midpoint of boundary segment computed with area weighting interpolation scheme |
| V | velocity, volume |
| $We_j$ | jet Weber number, $V_j^2\, D_j/\beta$ |
| x | horizontal coordinate in rectangular coordinate system |

PRECEDING PAGE BLANK NOT FILMED

| | |
|---|---|
| $y$ | vertical coordinate in rectangular coordinate system |
| $Y$ | liquid height |
| $z$ | axial coordinate in cylindrical coordinate system |
| $\alpha$ | geometric parameter, $\alpha = 1.0$ in cylindrical coordinates and equals 0.0 in plane (cartesian) coordinates |
| $\delta r$ | incremental step in the r direction |
| $\delta z$ | incremental step in the z direction |
| $\beta$ | kinematic surface tension, $L^3 T^{-2}$ |
| $\epsilon$ | boundary sensing parameter |
| $\theta_m$ | mixing time, T |
| $\lambda$ | minimum mesh dimension, minimum of $\delta r$ or $\delta z$ |
| $\mu$ | dynamic viscosity |
| $\eta$ | ratio of lengths in defining surface pressures |
| $\upsilon$ | kinematic viscosity, $L^2 T^{-1}$ |
| $\rho$ | density |
| $\sigma$ | surface tension |
| $\xi$ | relaxation parameter |
| $\phi$ | true pressure normalized to unit density |
| $\psi$ | arbitrary pressure normalized to unit density (pseudopressure), $L^2 T^{-2}$ |
| $\omega$ | vorticity |

Superscripts

| | |
|---|---|
| k | iteration index |
| n | time cycle index |

Subscripts

| | |
|---|---|
| B | bottom |
| L | liquid |
| j | jet |
| N | identifier for primary cell under consideration |
| NL | left boundary of cell N |
| NB | bottom boundary of cell N |
| T | top |
| t | tank |

## REFERENCES


1. Bradshaw, R. D. and Kramer, J. L.: An Analytical Study of Reduced-Gravity Propellant Settling. NASA CR-134593, General Dynamics Convair Aerospace Report CASD-NAS-74-005, Contract NAS3-16772, February 1974.

2. Bradshaw, R. D.; and Kramer, J. L.: A Variable Grid SMAC Computer Code With Arbitrary Boundaries: ERIE. P5634, Convair Aerospace Report CASD-NAS-74-006, Contract NAS3-16772, February 1974.

3. Betts, W. S.: An Analytical Study of Reduced-Gravity Liquid Reorientation Using a Simplified Marker and Cell Technique. NASA CR-120944, General Dynamics Convair Aerospace Report GDCA-DDB71-003, NAS3-14361, August 1972.

4. Betts, W. S.: A SMAC Computer Code With Arbitrary Boundaries: HOPI. P5623, General Dynamics Convair Aerospace Report 632-1-85, NAS3-14361, 19 April 1972.

5. Amsden, A. A.; and Harlow, F. H.: The SMAC Method: A Numerical Technique for Calculating Incompressible Fluid Flows. Los Alamos Scientific Laboratory Report No. LA-4370, 17 February 1970.

6. Bradshaw, R. D., Kramer, J. L., and Zich, J. L.: A Variable Grid SMAC Computer Code Containing Arbitrary Boundaries and Surface Tension: ERIE. P5634A, Report CASD-NAS-76-016, Contract NAS3-18739, April 1976.

7. Viecelli, J. A.: A Computing Method for Incompressible Flows Bounded by Moving Walls. Lawrence Radiation Laboratory Report UCRL-72815, September 1970.

8. Daly, B. J.: Numerical Study of the Effect of Surface Tension on Interface Instability. The Physics of Fluids, Vol. 12, No. 7, July 1969, pp 1340-54.

9. Daly, B. J.: A Technique for Including Surface Tension Effects in Hydrodyanmic Calculations. J. Computation Physics, Volume 4, 1969, pp 97-117.

10. Amsden, A. A.: Numerical Calculation of Surface Waves: A Modified Zuni Code With Surface Particles and Partial Cells. Los Alamos Scientific Laboratory Report No. LA-5146, May 1973.

11. Hastings, L. J.; and Rutherford, R.: Low Gravity Liquid-Vapor Interface Shapes in Axisymmetric Containers and a Computer Solution. NASA TMX-5379, October 7, 1968.

12. Concus, P., et al: Small Amplitude Lateral Sloshing in Spherical Containers Under Low Gravitational Conditions. NASA CR-72500, LMSC-A944673, NAS3-9704, Feb. 4, 1969.

13. Erickson, R.; and Lee, C. W.: Zero Gravity Venting and Mixing. General Dynamics Convair Report CASD-ERR-75-043, December 1975.

14. Fossett, H.; and Prosser, L. E.: The Application of Free Jets to the Mixing of Fluids in Bulk. Proc. Inst. Mech. Engr. (London), 160, 224 (1949).

15. Fox, E. A.; and Gex, V. E.: Single-Phase Blending of Liquids. A.I.Ch.E. Journal 2, 539 (1956).

16. Okita, N.; and Oyama, Y.: Chem. Eng. (Tokyo) 27, 252 (1963).

17. Poth, L. J., et al: A Study of Cryogenic Propellant Stratification Reduction Techniques, Annual Report. Vol. 1, FZA-419-1, p. 165, NAS8-20330, 15 September 1967.

18. Aydelott, J.: Personal communication, November 1975.

19. Abramovich, G. N.: "The Theory of Turbulent Jets." p. 512, MIT Press, Cambridge, Mass., 1963.

# DISTRIBUTION LIST - NAS3-17839

| Name | No. of Copies |
|---|---|
| National Aeronautics & Space Administration<br>Lewis Research Center<br>21000 Brookpark Road<br>Cleveland, OH 44135 | |
| Attn: Contracting Officer, MS 500-313 | 1 |
| E. A. Bourke, MS 500-205 | 5 |
| Technical Utilization Office, MS 3-16 | 1 |
| Technical Report Control Office, MS 5-5 | 1 |
| AFSC Liaison Office, MS 501-3 | 2 |
| Library, MS 60-3 | 2 |
| Office of Reliability & Quality Assurance, MS 500-211 | 1 |
| W. J. Masica, Project Manager, MS 500-318 | 30 |
| National Aeronautics & Space Administration<br>Headquarters<br>Washington, D.C. 20546 | |
| Attn: Office of Aeronautics & Space Technology | |
| Director, Manned Space Technology/RS | 1 |
| Director, Space Propulsion & Power/RP | 1 |
| F. W. Stephenson/RPI | 1 |
| Office of Manned Space Flight | |
| Director, Advanced Manned Mission/MT | 1 |
| Office of Space Science | |
| Director, Planetary Programs/SL | 1 |
| Director, Launch Vehicles & Propulsion/SV | 1 |
| NASA Scientific & Technical Information Facility<br>P.O. Box 33<br>College Park, MD 20740<br>Attn: NASA Representative | 10 |
| National Aeronautics & Space Administration<br>Ames Research Center<br>Moffett Field, CA 94035<br>Attn: Library | 1 |
| National Aeronautics & Space Administration<br>Flight Research Center<br>P.O. Box 273<br>Edwards, CA 93523<br>Attn: Library | 1 |
| National Aeronautics & Space Administration<br>Goddard Space Flight Center<br>Greenbelt, MD 20771<br>Attn: Library | 1 |
| National Aeronautics & Space Administration<br>John F. Kennedy Space Center<br>Cocoa Beach, FL 32931<br>Attn: Library | 1 |
| DD-MDD-43/F. S. Howard | 1 |
| DD-SED-4/W. H. Boggs | 1 |
| National Aeronautics & Space Administration<br>Langley Research Center<br>Hampton, VA 23365<br>Attn: Library | 1 |
| National Aeronautics & Space Administration<br>Johnson Space Center<br>Houston, TX 77001<br>Attn: Library | 1 |
| EP2/Z. D. Kirkland | 1 |

| Name | No. of Copies |
|---|---|
| National Aeronautics & Space Administration<br>George C. Marshall Space Flight Center<br>Huntsville, AL 35812<br>Attn: Library | 1 |
| ASTN-PF/A. L. Worlund | 1 |
| S&E-ASTN-PFA/L. Hastings | 1 |
| S&E-ASTN-DDS/F. Bugg | 1 |
| Aerospace Corporation<br>2400 East El Segundo Boulevard<br>Los Angeles, CA 90045<br>Attn: Library - Documents | 1 |
| Aeronautical Systems Division<br>Air Force Systems Command<br>Wright-Patterson Air Force Base<br>Dayton, OH 45433<br>Attn: Library | 1 |
| Air Force Office of Scientific Research<br>Washington, D.C. 20333<br>Attn: Library | 1 |
| Arthur D. Little, Inc.<br>20 Acorn Park<br>Cambridge, MA 02140<br>Attn: Library | 1 |
| Beech Aircraft Corporation<br>Boulder Facility<br>Box 631<br>Boulder, CO 80302<br>Attn: Library | 1 |
| Bell Aerosystems, Inc.<br>Box 1<br>Buffalo, NY 14240<br>Attn: Library | 1 |
| Boeing Company<br>Space Division<br>P.O. Box 3999<br>Seattle, WA 98124<br>Attn: Library | 1 |
| Dr. Wayne Patterson, MS82-94 | 1 |
| Chrysler Corporation<br>Space Division<br>P.O. Box 29200<br>New Orleans, LA 70129<br>Attn: Library | 1 |
| Defense Documentation Center<br>Cameron Station - Building 5<br>5010 Duke Street<br>Alexandria, VA 22314<br>Attn: TISIA | 1 |
| Denver-Division<br>Martin-Marietta Corporation<br>P.O. Box 179<br>Denver, CO 80201<br>Attn: Library | 1 |
| R. Page | 1 |

| Name | No. of Copies |
|---|---|
| Florida Institute of Technology<br>Space Technology Department<br>Melbourne, FL 32901<br>Attn: Dr. T. E. Bowman | 1 |
| Grumman Aircraft Engineering Corporation<br>Bethpage, Long Island, NY 11714<br>Attn: Library | 1 |
| Heat Transfer & Thermodynamic Laboratory<br>University of Michigan<br>Ann Arbor, MI 48107<br>Attn: Dr. John A. Clark | 1 |
| IIT Research Institute<br>Technology Center<br>Chicago, IL 60616<br>Attn: Library | 1 |
| Dr. Edward B. Igenbergs<br>8000 Muchen 80<br>*Rauchstrasse* 3<br>Germany | 1 |
| Jet Propulsion Laboratory<br>4800 Oak Grove Drive<br>Pasadena, CA 91103<br>Attn: Library | 1 |
| John Carroll University<br>Department of Physics<br>University Heights, OH 44118<br>Attn: Dr. E. F. Carome | 1 |
| Lawrence Berkeley Laboratory<br>Berkeley, CA 94720<br>Attn: 90-3108/P. Concus | 1 |
| Lawrence Radiation Laboratory<br>P.O. Box 808<br>Livermore, CA 94550<br>Attn: J. Viecelli | 1 |
| Linde, Division of Union Carbide<br>P. O. Box 44<br>Tonawanda, NY 11450<br>Attn: G. Niles | 1 |
| Lockheed Missiles and Space Company<br>P.O. Box 504<br>Sunnyvale, CA 94087<br>Attn: Library<br>G. D. Bizzell | 1<br>1 |
| Los Alamos Scientific Laboratory<br>P.O. Box 1663<br>Los Alamos, NM 87544<br>Attn: Dr. Francis H. Harlow<br>C. W. Hirt | 1<br>1 |
| Missiles and Space Systems Center<br>General Electric Company<br>Valley Forge Space Technology Center<br>P.O. Box 8555<br>Philadelphia, PA 19101<br>Attn: Library | 1 |
| National Science Foundation, Engr. Div.<br>1800 G. Street, N.W.<br>Washington, D.C. 20540<br>Attn: Library | 1 |
| Northrop Space Laboratories<br>3401 West Broadway<br>Hawthorne, CA 90250<br>Attn: Library | 1 |
| Office National D'Etudes Et De Recherches Aerospatiales<br>29, Avenue de la Division LeClerc<br>92 Chatillon<br>France<br>Par Jean Maulard<br>Michel Delattre | 1<br>1 |
| RCS/AED<br>P.O. Box 800<br>Princeton, NJ 08540<br>Attn: Mr. Daniel Balzer | 1 |
| Southwest Research Institute<br>Department of Mechanical Sciences<br>P.O. Drawer 28510<br>San Antonio, TX 78284<br>Attn: H. Norman Abramson<br>Franklin T. Dodge | 1<br>1 |
| Space and Information Systems Division<br>North American Rockwell<br>12214 Lakewood Boulevard<br>Downey, CA 90241<br>Attn: Library<br>D. Gluck | 1<br>1 |
| TRW Systems, Inc.<br>1 Space Park<br>Redondo Beach, CA 90278<br>Attn: Tech. Lib. Doc. Acquisitions | 1 |